



Hurricane impacts in the United States East Coast offshore wind energy lease areas

Kelsey B. Thompson¹, Rebecca J. Barthelmie², Sara C. Pryor¹

¹Department of Earth and Atmospheric Sciences, Cornell University, Ithaca, NY 14853, USA

5 ²Sibley School of Mechanical and Aerospace Engineering, Cornell University, Ithaca, NY 14853, USA

Correspondence to: Kelsey B. Thompson (kbt32@cornell.edu)

Abstract. Wind turbines deployed in offshore wind energy lease areas along the U.S. East Coast could significantly contribute to the national electricity supply. This region is also impacted by powerful tropical and extra-tropical cyclones that may lead to high structural loading on wind turbines and support structures and, in the event of above cut-out wind speeds, low power production (capacity factors < 0.2). Four sets of high-resolution simulations are performed for two category 3 tropical cyclones that tracked close to current offshore wind energy lease areas to assess the possible impacts on, and from, wind turbines. Simulations of Hurricanes Irene and Sandy are performed at convective permitting resolution with both the Weather Research and Forecasting Model (WRF) and the Coupled Ocean-Atmosphere-Wave-Sediment Transport (COAWST) Model to characterize geophysical conditions of relevance to offshore wind turbines. These simulations are performed without and with a wind farm parameterization (WFP) active with the latter using the assumption that existing lease areas are fully populated with 15 MW wind turbines at a 1.85 km spacing. Many aspects (e.g., track, near-surface wind speed, sea level pressure, precipitation volumes) are well reproduced in control simulations (no WFP) with both WRF and COAWST particularly for Hurricane Sandy. COAWST simulations lead to more intense cyclones with a slightly larger area of storm-force wind speeds, a higher likelihood of hub-height wind speeds > 25 m s⁻¹, plus higher precipitation volumes, possibly indicating under-estimation of hurricane risk in uncoupled simulations. All eight simulations indicate maximum hub-height wind speeds (HH WS) within the existing lease areas below 50 m s⁻¹. However, COAWST simulations indicate frequent wind-wave misalignment of > 30° and the joint occurrence of significant wave height, hub-height wind speed, and wave period in some lease areas reach levels that are likely to be associated with large structural loads. This work re-emphasizes the utility of coupled simulations in describing geophysical conditions of relevance to offshore wind turbine operating conditions.

1 Introduction

1.1 Motivation

At the end of 2023, the global offshore wind energy installed capacity (IC) was approximately 75.2 GW (GWEC, 2024a) due in part to a 24% increase in installed capacity during 2023 (GWEC, 2024b). The plentiful offshore wind resource (Marvel et al., 2013; Bodini et al., 2024; Pryor and Barthelmie, 2024b) and recent reductions in the Levelized Cost of Energy for offshore deployments (Jansen et al., 2020; Wiser et al., 2021) mean that the number of wind turbines (WT) deployed in (coastal) offshore regions is projected to rapidly increase (GWEC, 2024b; Pryor and Barthelmie, 2024b).

The offshore environment presents significant challenges for making long-term, climatologically representative robust measurements of properties such as wind speed at wind turbine hub-height (HH WS) (Foody et al., 2024) that are critical for determining the wind resource and key aspects of operating conditions (IEC, 2019b, a; Mudd and Vickery, 2024). The relative paucity of measurements leads to financial uncertainty and thus potentially jeopardizes realizing U.S. national goals for achieving the energy transition (Hansen et al., 2024). It also means that numerical modeling is playing a critical role in



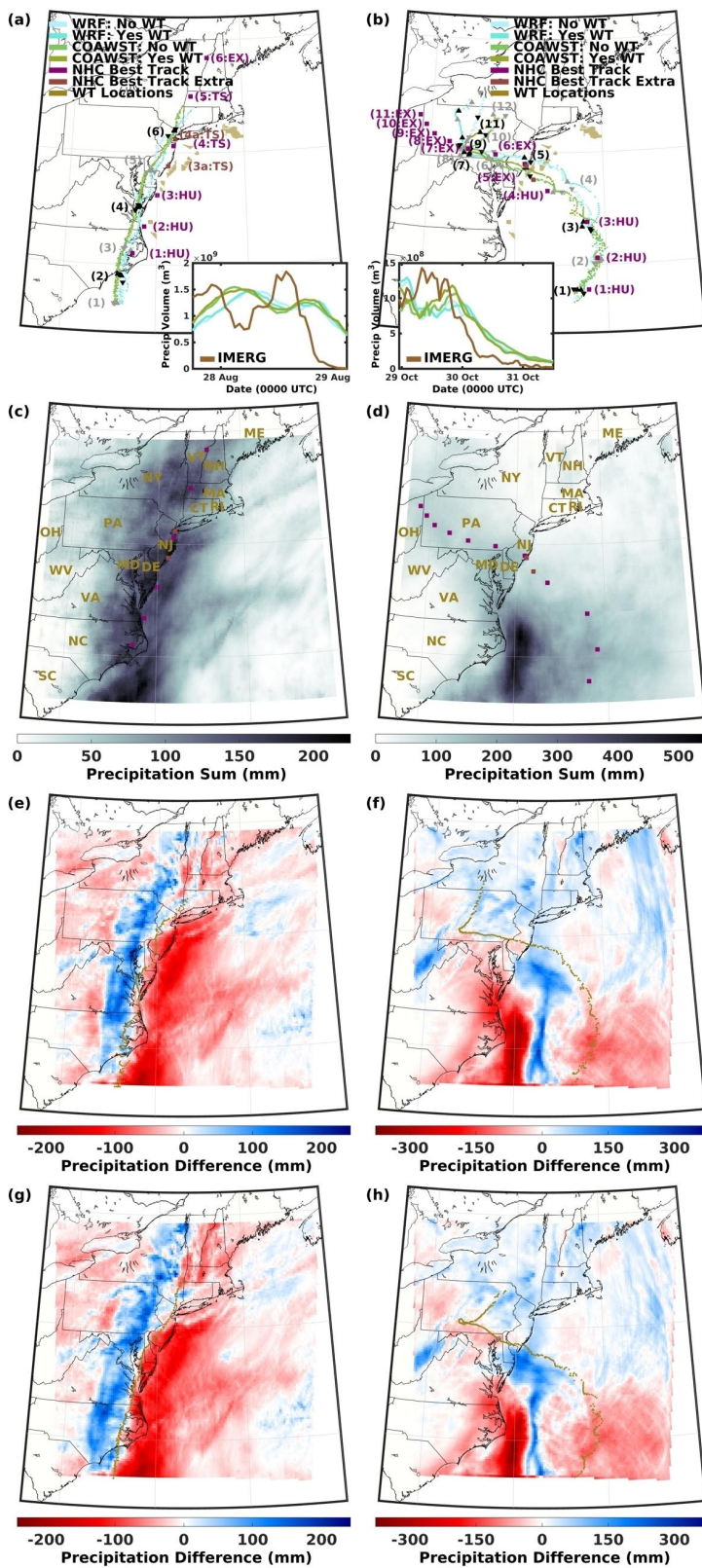
projecting wind resource and operating conditions in offshore wind energy development areas (Kresning et al., 2020; Pryor
40 and Barthelmie, 2021; Bodini et al., 2024; Pryor and Barthelmie, 2024b; Wang et al., 2024).

Substantial offshore wind energy developments are planned or in progress along the U.S. East Coast (Fig. 1) in regions with
high wind resource (power generation potential), close proximity to major demand centers, and shallow water depths (Pryor
et al., 2021; Pryor and Barthelmie, 2024b, a). This region also has the potential to be impacted by tropical cyclones and/or
45 transitioning tropical-extratropical cyclones (Xie et al., 2005; Baldini et al., 2016; Barthelmie et al., 2021; Wang et al.,
2024).

Wind speeds within tropical cyclones frequently exceed the threshold at which wind turbines cease power production (25-30
m s⁻¹) to avoid high operational loads (Petrović and Bottasso, 2014). There are reports of individual wind turbine failures
50 during hurricanes (Chen and Xu, 2016), and six wind turbines in a wind farm without hurricane-resistant wind turbines were
damaged by 65 m s⁻¹ wind speeds during Typhoon Yagi in September 2024 (Yihe, 2024). Accordingly, hurricane-induced
extreme wind conditions represent an important component of wind turbine design standards (IEC, 2019b, a; Ju et al., 2021;
Martín del Campo et al., 2021). For offshore wind farm lease areas (LA) in coastal waters along the U.S. East Coast (Fig. 1),
past research has suggested areas north of Maryland have the lowest risk of hurricane damage (< 5% probability that in a 20
55 year period more than 10% of the wind turbines would be destroyed) (Rose et al., 2012b, a). Offshore LA near North
Carolina experienced fewer than 40 instances of hurricane force winds (10-m wind speeds > 33 m s⁻¹) between 1900 and
2013, while those located near Maryland and farther northward experienced ~ 20 instances (Hallowell et al., 2018). Based on
output from the 30 km resolution ERA5 gridded dataset, the highest 50-year return period (RP) wind speed (WS) at 100 m
above sea level (a.s.l.) and significant wave heights (Hs, i.e., the mean height – crest to trough of the largest one-third of
60 waves) for the U.S. East Coast offshore wind energy LA are ~ 39.7 m s⁻¹ and ~ 11 m, respectively (Barthelmie et al., 2021).
Equivalent estimates from buoy measurements are; 32.6 m s⁻¹ and 9.5 m (Kresning et al., 2024). A further model-based study
indicated 50-year RP Hs of 9-11 m for the northernmost LA considered here (McElman et al., 2024).

Wind-wave coupling plays a key role in both near-surface atmospheric processes and wind turbine loading (Valamanesh et
65 al., 2013; Valamanesh et al., 2015; Koukoura et al., 2016; Hallowell et al., 2018; Hashemi et al., 2021; Li et al., 2022; Müller
et al., 2024). Analyses based on buoy-based measurements of wind and waves along the U.S. East Coast indicated the mean
failure probability during a 20-year wind turbine lifetime is 9.6×10^{-6} for a functional wind turbine yaw control system and
 2.9×10^{-4} for a non-functional yaw control system (Hallowell et al., 2018). Wind-wave directional offset is also considered
in offshore wind turbine design codes (IEC61400-3) for loading on the support structure (IEC, 2019a). A 90° wind-wave
70 misalignment is projected to increase the mud-line bending moment for a monopile foundation by up to a factor of five, and
even more modest misalignment of 30° approximately doubles this bending moment (Fischer et al., 2011). This
amplification of bending moment with wind-wave misalignment is greatly enhanced under high HH WS (Stewart and
Lackner, 2014).

75





80 **Figure 1: Hurricane Irene (left) and Hurricane Sandy (right). (a, b) Hurricane tracks from model simulations presented herein**
 (WRF without the action of wind turbines, WRF with the action of wind turbines, COAWST without the action of wind turbines,
 and COAWST with the action of wind turbines), derived from minimum SLP every 10 min and the corresponding NHC “best
 track” locations. HU indicates hurricane stage, TS indicates tropical storm stage, and EX indicates extratropical stage. Numbers
 in brackets represent the location at the times specified in Table 1. The time series plots are the 1-h precipitation volume within
 85 375 km from the track location for each simulation and IMERG V07. (c, d) Accumulated IMERG V07 precipitation during
 the entire simulation period (1200 UTC on 24 August 2011 through 1200 UTC on 29 August 2011 and 1200 UTC on 25 October 2012
 through 1200 UTC on 1 November 2012, respectively) and NHC best track locations (from (a) and (b)). Also shown are the U.S.
 state abbreviations; Maine (ME), New Hampshire (NH), Vermont (VT), Massachusetts (MA), Rhode Island (RI), Connecticut
 90 (CT), New York (NY), New Jersey (NJ), Pennsylvania (PA), Ohio (OH), West Virginia (WV), Maryland (MD), Delaware (DE),
 Virginia (VA), North Carolina (NC), and South Carolina (SC). (e, f) Difference in accumulated precipitation (WRF without the
 action of wind turbines minus IMERG) and the hurricane track from the WRF no WT simulation (every 10 min). (g, h) Difference
 in accumulated precipitation (COAWST without the action of wind turbines minus IMERG) and the hurricane track from the
 COAWST no WT simulation (every 10 min).

95 **Table 1: The time (UTC) and date that correspond to the numbered locations for Hurricanes Irene and Sandy shown in Fig. 1. All
 dates for Irene are in 2011 and all dates for Sandy are in 2012.**

location	Irene time and date	Sandy time and date
1	1800 27 Aug	0000 29 Oct
2	0000 28 Aug	0600 29 Oct
3	0600 28 Aug	1200 29 Oct
3a	0935 28 Aug (landfall at Brigantine Island, NJ)	-
4	1200 28 Aug	1800 29 Oct
4a	1300 28 Aug (landfall at Coney Island, NY)	2100 29 Oct (downgraded to extratropical)
4b	-	2330 29 Oct (landfall at Brigantine Island, NJ)
5	1800 28 Aug	0000 30 Oct
6	0000 29 Aug	0600 30 Oct
7	-	1200 30 Oct
8	-	1800 30 Oct
9	-	0000 31 Oct
10	-	0600 31 Oct
11	-	1200 31 Oct
12	-	1800 31 Oct

100 Estimation of design criteria extreme wind speeds from numerical modeling is critically dependent on the grid spacing at
 which the model is applied (Larsén et al., 2012) and momentum dissipation at the ocean surface which in turn is determined
 by wind-wave coupling and the parameterization used to dictate the surface roughness length (Larsén et al., 2019; Wang et
 al., 2024). The Coupled Ocean-Atmosphere-Wave-Sediment Transport (COAWST) modeling system (Warner et al., 2010)
 comprises a series of linked model components. In the research presented herein these models are; the Weather Research and
 Forecasting Model (WRF) (Skamarock et al., 2019), the Regional Ocean Modeling System (ROMS) (Shchepetkin and
 105 McWilliams, 2005; Haidvogel et al., 2008; Shchepetkin and McWilliams, 2009), and Simulating Waves Nearshore (SWAN)
 (Booij et al., 1999) and they interact through use of the Model Coupling Toolkit (MCT) (Jacob et al., 2005; Larson et al.,
 2005; Warner et al., 2008).



110 Only limited previous research has sought to quantify the degree to which wind-wave coupling improves simulation fidelity
and/or intensity for wind speeds at heights of relevance to offshore wind turbines. One such study focused on 23 intense
cyclones in the North Sea and found that when WRF is coupled to SWAN through a wave boundary layer model with an
innermost domain with grid spacing of 2 km, the inferred 50-year RP wind speeds were systematically higher than those
from WRF alone and the degree of agreement in extreme wind speeds at five offshore and/or coastal masts was improved
(Larsén et al., 2019). A further study found that for Tropical Storm Ana in the mid-Atlantic Bight, two-way coupled WRF
115 and WaveWatch III (WW3) simulated peak 90-m wind speeds were a closer match to observations than the corresponding
values from either a standalone WRF or one-way coupled WRF simulation (Gaudet et al., 2022). Simulation of Hurricane
Sandy with WRF with FVCOM (the unstructured-grid, Finite-Volume Community Ocean Model) coupled through the Earth
System Model Framework also found improved agreement with observations for the central pressure location and intensity
plus 10-m wind speeds relative to simulation solely with WRF (Li and Chen, 2022). COAWST (configured with WRF 3.2,
120 ROMS 3.3, and SWAN 40.81) coupled with MCT showed “modest improvement in track but significant improvement in
intensity ... versus uncoupled (e.g., standalone atmosphere, ocean, or wave) model simulations” for Hurricane Ivan
(Zambon et al., 2014a). Thus, there is provisional evidence that, in accord with expectations, detailed coupling of the
atmosphere-wave and ocean models improves simulation of atmospheric parameters within these extreme events relative to
simulations with WRF alone.

125
In addition to the importance of intense cyclones (e.g., hurricanes) to wind turbine design standards, there have also been
suggestions that very wide-spread deployment of offshore wind turbines in the U.S. coastal zone could aid in reducing the
intensity of tropical cyclones and thus reduce damage onshore (Jacobson et al., 2014). Simulations of three hurricanes using
the GATOR-GCMOM model indicated that offshore wind turbine arrays comprising 110,000 and 420,000 wind turbines
130 (installed capacities > 300 GW) at installed capacity densities (ICD) of 8 – 17 MW km⁻² might reduce 15-m wind speeds by
over 25 m s⁻¹ and reduce storm surge by up to 79% (Jacobson et al., 2014). Simulations with 22,000 to 74,000 wind turbines
also suggested that offshore wind turbines could reduce the amount of precipitation over land, downstream of the wind farms
(Pan et al., 2018).

1.2 Objectives

135 Research presented herein uses storyline simulations of two of the most powerful hurricanes that have occurred within the
U.S. East Coast coastal waters in which offshore wind energy LA have been auctioned (Fig. 1, see further details in Figs. S1-
S2). Four sets of simulations are performed for each of these hurricanes; (a) WRF, (b) WRF with the action of wind turbines
included in offshore wind energy lease areas purchased prior to mid-2023, (c) COAWST, and (d) COAWST with the action
of wind turbines included. Our specific research questions are as follows:

- 140
- 1) Are the characteristics of these hurricanes well captured using either the WRF or COAWST models? A sub-
component of this question is does the more explicit coupling in COAWST improve simulation fidelity?
 - 145 2) Do these simulations suggest that either of these hurricanes would have been characterized by either (a) widespread
loss of power production across these lease areas due to cut-out at high wind speeds and for how long and/or (b)
exceedance of wind turbine design wind speeds and/or very high wind-wave structural loading? Again, a sub-
component of this question is does use of COAWST versus WRF change wind speed intensity and/or the duration
of time with low power production?



- 150 3) If wind turbine rotor extraction of momentum is simulated using a wind farm parameterization in WRF and
COAWST, is there evidence of weakening of the hurricanes for wind turbine numbers and installed capacity
densities that are likely to be achieved using the offshore wind energy lease areas considered here?

2 Data and Methods

2.1 Characteristics of the hurricanes considered herein

155 Research presented herein focuses on two recent hurricanes:

- 1) Hurricane Irene became a category 3 hurricane, with 54 m s^{-1} wind speeds at 10-m height in the Bahamas at 1200 UTC on 24 August 2011 (Avila and Cangialosi, 2011). It made landfall at Cape Lookout, North Carolina at 1200 UTC on 27 August with 39 m s^{-1} 10-m wind speeds. After moving out over the water, it again made landfall, this
160 time as a tropical storm, with 31 m s^{-1} wind speeds reported at Brigantine, New Jersey at 0935 UTC 28 August. The cyclone then moved over Coney Island, New York with 28 m s^{-1} wind speeds reported at 1300 UTC. Simulations presented herein are initialized at 1200 UTC on 24 August 2011 and run through 1200 UTC on 29 August 2011.
- 2) Hurricane Sandy became a category 3 hurricane, with 51 m s^{-1} wind speeds at 10-m height in eastern Cuba at 0525
165 UTC on 25 October 2012 (Blake et al., 2013; Lackmann, 2015). It grew to have a roughly 1611 km diameter of tropical-storm-force wind speeds, before making landfall near Brigantine, New Jersey as a post-tropical cyclone with 36 m s^{-1} 10-m wind speeds and a minimum pressure of 945 hPa at 2330 UTC 29 October. Simulations presented herein run from 1200 UTC on 25 October 2012 through 1200 UTC on 1 November 2012.

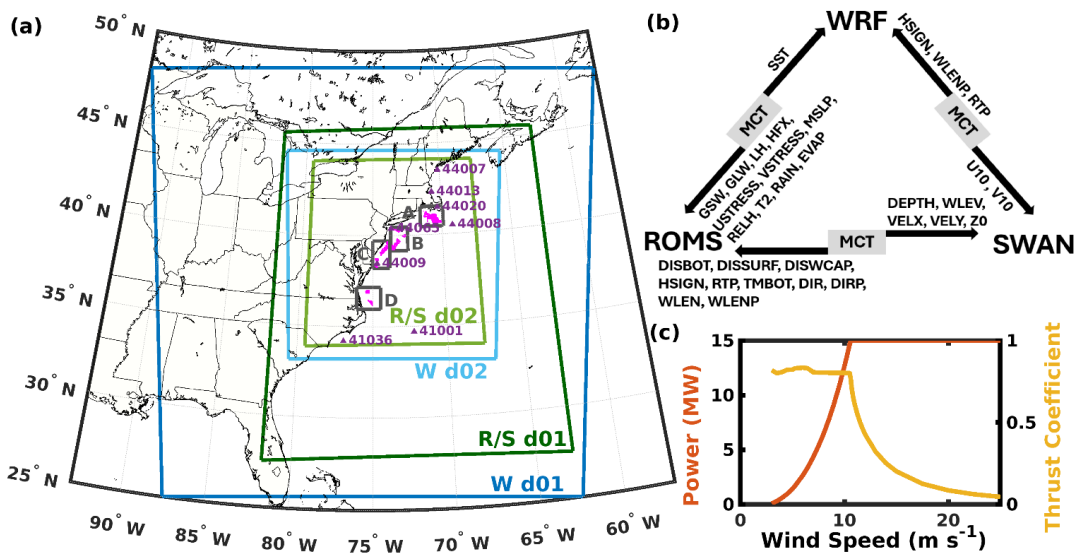
2.2 Modeling

170 The source of initial and lateral boundary conditions (Khaira and Astitha, 2023) and specific model configurations employed within WRF and COAWST (including the coupling system) have a critical impact on simulated flow conditions (Mooney et al., 2019). In this research, both WRF (v4.2.2) and COAWST (v3.7 and MCT v2.6.0) simulations use two domains (Fig. 2a) and the coupling interval in COAWST is 10 min (Fig. 2b). The source of boundary and initial conditions and key physics options (Tables 3 and 4) are informed by previous simulations of Hurricanes Sandy (Zambon et al., 2014b) and Irene
175 (Mooney et al., 2016). The MYNN2 planetary boundary layer scheme is used due to the compatibility with the Fitch wind-farm parameterization (WFP) (Fitch et al., 2012) that is used here to compute power production, momentum extraction, and turbulent kinetic energy (TKE) induced by the action of wind turbines. Following previous research (Pryor and Barthelmie, 2024b, a), we assume that all auctioned offshore lease areas along the U.S. East Coast shown in Fig. 2a are populated with IEA reference 15 MW wind turbines (Fig. 2c) with a spacing of 1.85 km for an average ICD of 4.3 MW km^{-2} . This results in
180 a total of 2642 wind turbines (Fig. 2a), each of which has a hub height of 150 m, and a rotor diameter of 240 m. The 1.85 km wind turbine spacing and 1.33 km WRF domain 02 (d02) grid spacing (dx) results in 2641 grid cells with at least one wind turbine; one grid cell has two wind turbines. Of the 71 unstaggered WRF vertical levels, level 15 has a mean height of 155 m in grid cells with wind turbines and is therefore used for HH WS. Note the wind speeds output from d02 are for a nominal model time step of 2 s but are representative of a spatial average of 1.33 km by 1.33 km, while the design standards are for a
185 sustained wind speed at a point (Larsén and Ott, 2022).

Variation of wave state and surface roughness length with wind speed is an important determinant of extreme, near surface wind speeds and turbulence intensity (Zambon et al., 2014a; Porchetta et al., 2019; Porchetta et al., 2020; Porchetta et al., 2021; Wang et al., 2024). The COAWST simulations are configured using the Taylor Yelland formulation (Taylor and



190 Yelland, 2001) to calculate surface roughness length following past research (Zamboni et al., 2014b) that found use of this
 parameterization resulted in better fidelity for Hurricane Sandy track, intensity, sea surface temperatures, and wave heights
 than alternatives (Oost et al., 2002; Drennan et al., 2005). Use of the MYNN surface layer with WRF and the
 DRAGLIM_DAVIS drag limiter option with COAWST, means all simulations implement a maximum ocean roughness drag
 coefficient of 2.85×10^{-3} , consistent with research that has shown asymptotic behavior of drag at high wind speeds (Davis et
 195 al., 2008). Data are output every 10 min and each simulation is subject to a warm restart every 6 h due to wall clock
 limitations on the compute platform.



200 **Figure 2:** (a) Domains 01 and 02 (d01 and d02) for WRF (W), ROMS (R), and SWAN (S) and locations of offshore wind energy LA
 considered herein (in the simulations with wind turbines, these LA contain 2642 wind turbines which are shown in magenta). Also
 shown are the eight NDBC buoys used in the simulation evaluation. (b) Schematic of information flow among the COAWST model
 components. See Table 2 for additional details. (c) Power and thrust coefficient for the 15 MW IEA reference wind turbine
 (Gaertner et al., 2020).

205

210

215



220 **Table 2: Additional details about the information flow among the COAWST model components in Fig 2b.**

name	abbreviation	units
depth below mean sea level	DEPTH	m
mean wave direction	DIR	rad
peak wave direction	DIRP	rad
energy dissipation due to bottom friction	DISBOT	$W m^{-2}$
energy dissipation due to surf breaking	DISSURF	$W m^{-2}$
energy dissipation due to white-capping	DISWCAP	$W m^{-2}$
evaporation rate	EVAP	$kg m^{-2} s^{-1}$
downward long wave flux at ground surface	GLW	$W m^{-2}$
net short wave flux at ground surface	GSW	$W m^{-2}$
upward heat flux at the surface	HFX	$W m^{-2}$
significant wave height	HSIGN	m
latent heat flux at the surface	LH	$W m^{-2}$
mean sea level pressure	MSLP	mb
rainfall rate	RAIN	$kg m^{-2} s^{-1}$
relative humidity	RELH	-
relative peak period	RTP	s
sea surface temperature	SST	K
temperature at 2 m	T2	$^{\circ}C$
near bottom wave period	TMBOT	s
x-wind component at 10 m	U10	$m s^{-1}$
surface u-stress	USTRESS	$N m^{-2}$
y-wind component at 10 m	V10	$m s^{-1}$
current velocity component in x direction	VELX	$m s^{-1}$
current velocity component in y direction	VELY	$m s^{-1}$
surface v-stress	VSTRESS	$N m^{-2}$
mean wave length	WLEN	m
peak wave length	WLENP	m
water level	WLEV	m
roughness length	Z0	m

225

230



Table 3: Sources of initial and boundary conditions for WRF and COAWST.

WRF (version 4.2.2)	
Atmosphere:	North American Mesoscale Forecast System (NAM; 12 km, 6 h)
Sea Surface Temperature:	Group for High Resolution Sea Surface Temperature (GHRST) Level 4 Operational Sea Surface Temperature and Sea Ice Analysis (OSTIA) (OSTIA-UKMO-L4-GLOB-v2.0; 0.05°, 24 h)
Horizontal resolution:	4 km for d01, 1.33 km for d02
Model top / # vertical levels:	50 hPa / 72
Time step (dt):	6 s for d01, 2 s for d02
ROMS (version 3.9)	
Coastlines:	Global Self-consistent, Hierarchical, High-resolution Geography Database (GSHHG; full resolution)
Bathymetry (also for SWAN):	General Bathymetric Chart of the Oceans (GEBCO) 2022 (15 arc-second)
3D boundary conditions, initial conditions, and climatology:	HYbrid Coordinate Ocean Model (HYCOM GLBa0.08 expt 90.9)
2D boundary conditions (tides):	Advanced Three-Dimensional Circulation Model (ADCIRC 2001v2e)
Horizontal resolution:	10 km for d01, 3.33 km for d02
Time step (baroclinic / barotropic):	1.5 s (d01), 0.5 s (d02) / 30 (d01 & d02)
# vertical levels	25
SWAN (version 41.31)	
Wind forcing:	Global Forecast System (GFS): 0.5°, 6 h
Boundary conditions:	parametric forcing file (TPAR): 30 min WaveWatch III (WW3) data
Horizontal resolution:	10 km for d01, 3.33 km for d02
Time step:	12 s for d01, 4 s for d02
Frequency range:	0.04 to 1.0

235

Table 4: Physics settings used with WRF and COAWST simulations.

Model physics	Key reference(s)
microphysics: WRF single-moment 6-class scheme (WSM6)	(Hong and Lim, 2006)
longwave radiation: Rapid Radiative Transfer Model (RRTM)	(Mlawer et al., 1997)
shortwave radiation: Dudhia scheme (MM5)	(Dudhia, 1989)
surface layer: MYNN	(Olson et al., 2021)
land surface: Unified Noah land surface model	(Chen and Dudhia, 2001b, a; Ek et al., 2003; Tewari et al., 2004)
planetary boundary layer: Mellor-Yamada Nakanishi and Niino Level 2.5 (MYNN2)	(Nakanishi and Niino, 2006)
cumulus param.: Kain-Fritsch (d01; none for d02)	(Kain, 2004)
wind farm param. (both domains)	(Fitch et al., 2012)



240 2.3 Evaluation data sets

Critical aspects of the WRF and COAWST simulations without the action of wind turbines are evaluated using:

- 245 (i) National Hurricane Center (NHC) “best track” information and wind radii maximum extent data from Tropical Cyclone Reports (Avila and Cangialosi, 2011; Blake et al., 2013) and the Atlantic hurricane database (HURDAT2; (Landsea and Franklin, 2013)).
- (ii) 30-minute precipitation at 0.1 degree resolution from the Integrated Multi-satellitE Retrievals for the Global Precipitation Measurement (GPM) mission (IMERG) V07 final run data set (Huffman et al., 2024).
- 250 (iii) National Data Buoy Center (NDBC) buoy-based measurements of wind speeds (WS), sea level pressure (SLP), sea surface temperature (SST), and significant wave height (Hs) (NDBC, 2009) (<https://www.ndbc.noaa.gov>) (see Fig. 2a). Note: The eight buoys from which data are presented are a mixture of 3-meter foam and 3-meter discus buoys. The anemometer and barometer heights vary between 3.8 and 4.1 m, and 2.4 and 3.4 m.

2.4 Analysis approach

255 Hurricane centroid locations are computed every 10 minutes as the minimum SLP after 3×3 smoothing is applied to the model output and are used for comparison with the NHC best track information. The initial tracking position is the first time step when the minimum SLP is fully within d02 and tracking continues until the implied translational speed/direction of motion between adjacent time steps is inconsistent with physical expectations in terms of direction or translational speed. Hurricane Irene is tracked for 33 h, from 1800 UTC 27 August 2011 through 0300 UTC 29 August 2011 and Hurricane

260 Sandy is tracked for 67 h, from 2300 UTC 28 October 2012 through 1800 UTC 31 October 2012 (Fig. 1). Evaluation relative to SLP and wind speed data from the NDBC buoys is performed using a search area of 3×3 grid cells. Evaluation of simulated precipitation relative to IMERG over all of d02 is performed after regridding output to the IMERG grid. The volume of water exhausted as precipitation from the tropical cyclone is computed using a search radius of 375 km (see examples in Fig. 3) around the cyclone centroid in the simulation output and from the best track locations applied to IMERG.

265

When evaluating hurricane impacts on wind turbines within the U.S. East Coast LA, analyses are presented for both all 2641 grid cells containing wind turbines, and four LA clusters defined as in (Pryor and Barthelmie, 2024b) and listed from north to south; A (1073 WT), B (662 WT), C (624 WT), and D (283 WT) (Fig. 2a). Because prior research has indicated the challenges in perfectly reproducing hurricane tracks, we consider conditions in both grid cells containing wind turbines and/or all ocean-based grid cells within the respective LA cluster area. To facilitate comparison across the LA clusters,

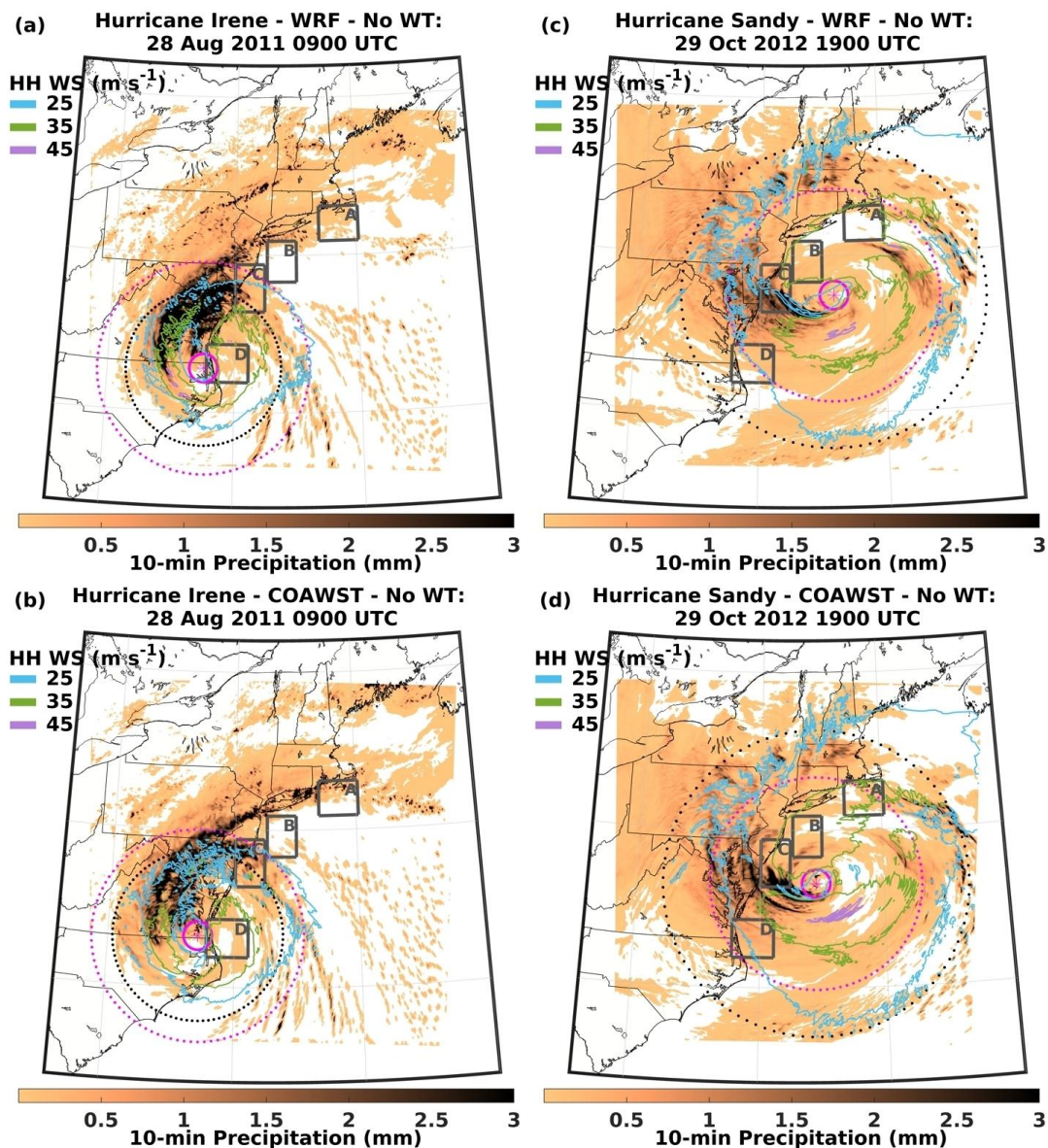
270 power production computed by the Fitch WFP is used to compute capacity factors (CF), which are the ratio of the power produced divided by that which would be produced if all wind turbines were operating at rated capacity (15 MW). System-wide CF < 0.2 are used here as an indicator of low power production.

275 Three-dimensional and joint occurrences of HH WS, Hs, and peak period (Tp) in WT-containing grid cells from the COAWST simulations are presented along with histograms of estimated wind-wave misalignment at the LA cluster centers in HH WS classes of $3 - < 10.6 \text{ m s}^{-1}$, $10.6 - 25 \text{ m s}^{-1}$, and $> 25 \text{ m s}^{-1}$, to represent high thrust, moderate thrust, and above rated wind speeds (Fig. 2c).



280 Three metrics are used to analyze the impact of wind turbines on hurricane intensity and are compared for simulations with
WRF and COAWST without and with the WFP active. The cumulative volume of precipitation within 375 km of the
minimum SLP and the mean wind speed at 500 hPa (approximately the level of non-divergence, e.g., (Riehl and Malkus,
1961)) computed for grid cells that lie 50-375 km from the centroid (i.e., beyond the likely eye radius) (Morin et al., 2024;
Müller et al., 2024) are used as metrics of intensity. The mean outermost radius of tropical storm force (R_{18} , 18 m s^{-1} , see
285 Fig. 3) wind speeds at 10-m computed using azimuth sectors of 10° (Powell and Reinhold, 2007) for all sectors where the
distance from the cyclone centroid to the d02 boundary is $\geq 200 \text{ km}$ is used as a measure of cyclone size. Mood's test
(Hettmansperger and Malin, 1975) is used to assess the statistical significance of differences in the median values of these
metrics.

290





295 **Figure 3: Simulated precipitation from WRF (a, c) and COAWST (b, d) during two example 10 minute periods (background color) and contours of HH WS at 25, 35, and 45 m s⁻¹ for 0900 UTC 28 August 2011 (a, b) and 1900 UTC October 2012 (c, d) when the hurricanes are close to wind turbine LA. Magenta rings mark 50 km and 375 km from the minimum SLP. The black rings mark R₁₈ radii of (a) 274 km, (b) 301 km, (c) 539 km, and (d) 541 km. For legibility, the colorbar is truncated. Maximum precipitation is (a) 14.0 mm, (b) 13.8 mm, (c) 18.4 mm, and (d) 16.8 mm.**

3 Results

3.1 Evaluation of the no-wind turbine simulations

300 Simulations of Hurricane Irene exhibit lower fidelity than those of Hurricane Sandy. The centroid of Hurricane Irene is consistently displaced west (further inland, Fig. 1a) than the NHC best track data, and the translational speed is also negatively biased in simulations with both WRF and COAWST. This bias is consistent with previous COAWST simulations of this hurricane performed with 12 km grid spacing and using a range of initial and lateral boundary conditions (Mooney et al., 2019). Simulation bias is also evident in comparison with buoy observations (Table 5, Fig. 4, and Figs. S3-S9) both in
305 terms of the magnitudes and timing of the maximum wind speeds and minimum SLP. The maximum near-surface wind speeds differ (model minus buoy observations) by between -4.2 and 0.7 m s⁻¹ (WRF at 2.6 m) and -3.2 and 6.0 m s⁻¹ (COAWST at 2.6 m). The displacement of the Hurricane Irene centroid in the simulations results in higher over land precipitation (by up to 209 mm in some IMERG grid cells) and negative bias offshore (Fig. 1). However, the volume of water vented from the hurricane is relatively well reproduced in the simulations. During the time of tracking, the mean (1-h)
310 precipitation volume within 375 km of the centroid is 9.87×10^8 m³ based on IMERG combined with the NHC best track data, while the corresponding values (and percent error) are 1.14×10^9 m³ (15.1% overestimation) and 1.18×10^9 m³ (19.9% overestimation), for the WRF and COAWST simulations, respectively (Fig. 1). Mean R₁₈ is 279 km in the WRF simulation but is larger by an average of 23 km in 192 of the 199 tracked 10-min positions in the COAWST simulation. These mean R₁₈ values are similar to, but smaller than, those reported at a 6-hrly interval from HURDAT2 based on analyses in four
315 quadrants (mean R₁₈ of 495 km in the SE quadrant and 157 km in the NW quadrant). The differences in R₁₈ and precipitation in these simulations versus HURDAT2 and IMERG are likely due to bias introduced by proximity to the d02 boundary in the simulation and differences in the fraction of the system over land (Chen and Yau, 2003) due to differences in storm tracks (Fig. 1).

320 As in past research (Zambon et al., 2014b), both the WRF and COAWST simulations of Hurricane Sandy exhibit good agreement with NHC best track data up to about 12 h after landfall in New Jersey (Fig. 1b). The mean distance between the centroids for locations; 1, 2, 3, 4, 4a, 4b, and 5 in Fig. 1b is 66.7 km (WRF) and 51.4 km (COAWST). For those seven times the distances of separation range from 30.3 to 129.1 km (WRF) and 12.0 to 71.1 km (COAWST). These positional offsets are smaller than those presented in previous research on, for example, cyclonic storm Ockhi (Mukherjee and Ramakrishnan,
325 2022) and the mean values from Tropical Storm Delta, Hurricane Ophelia, Hurricane Leslie, and Tropical Storm Theta (Calvo-Sancho et al., 2023). Consistent with expectations, agreement tends to degrade once the cyclone has made landfall as the system becomes less organized and more asymmetric (Zambon et al., 2014b). Modeled time series of SLP, SST, Hs, and wind speeds exhibit some level of agreement with the NDBC buoy observations in terms of time-variability (Table 6, Fig. 4, and Figs. S3-S9). As expected, due to spatial averaging and the difference in height, the maximum wind speeds from the
330 lowest model level (~ 2.6 m) are generally lower than the point observations on the buoys at 3.8 or 4.1 m. Seven of the eight values are smaller in the WRF simulation, and six of eight comparisons indicate lower values in the COAWST simulation. The maximum near-surface wind speeds (model minus buoy observations) differ by 3.1 to 9.0 m s⁻¹ (WRF) and 2.9 to 7.8 m s⁻¹ (COAWST). The mean absolute difference in minimum SLP is 3.1 hPa (WRF) and 2.6 hPa (COAWST). Significant wave



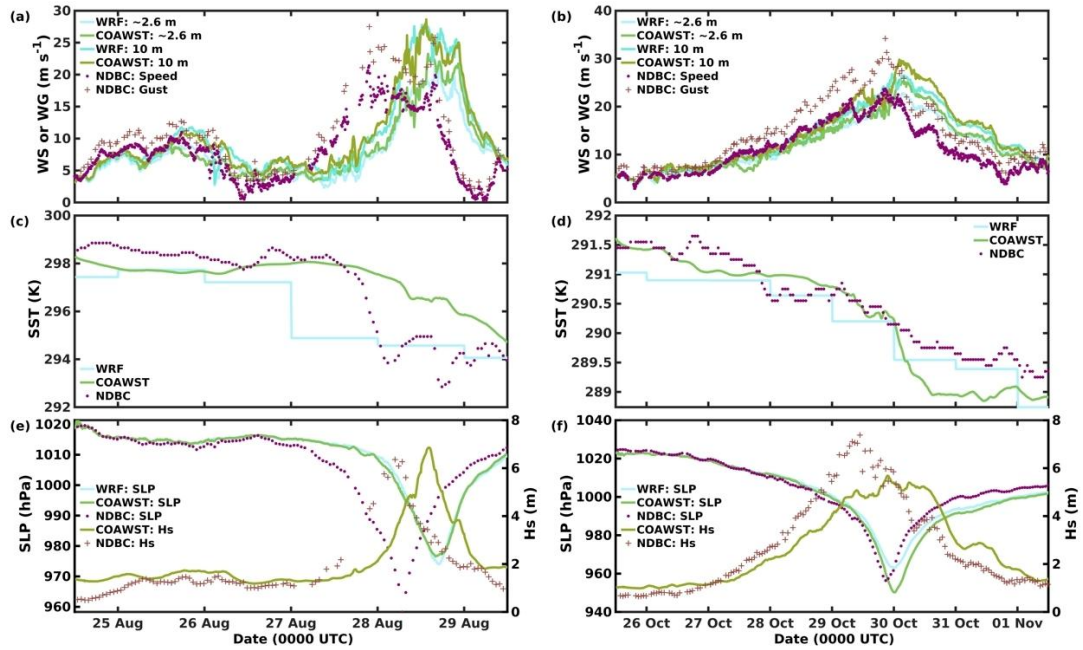
heights from COAWST are generally lower than those from the buoy observations, with a (model minus buoy observations) difference of -3.7 to 0.1 m (a bias of up to 37%). The spatial pattern of precipitation from the simulations exhibits some similarity with IMERG, although the centroid of the region of maximum precipitation is displaced westward (towards the coast of North Carolina) in IMERG relative to the WRF and COAWST simulations by approximately 125 km (Fig. 1). The volume of precipitation vented from the hurricane exhibits relatively good agreement between the simulations and IMERG. The mean (1-h) precipitation volume within 375 km from the centroid is $5.35 \times 10^8 \text{ m}^3$ based on IMERG combined with the NHC best track data, while the corresponding values (and percent error) are $5.82 \times 10^8 \text{ m}^3$ (+8.7%) and $5.83 \times 10^8 \text{ m}^3$ (+8.9%) for the WRF and COAWST simulations (Fig. 1). Mean R_{18} prior to landfall is 506 km in the WRF simulation and is larger by an average of 14 km in 119 of the 151 tracked 10-min positions in the COAWST simulation. The R_{18} estimates from 6-h HURDAT2 data before and after landfall are 705 km and 776 km and are larger than those from the WRF and COAWST simulation due to biases in the calculation when the hurricane extends beyond the d02 boundary.

345

Table 5: Comparison of WRF and COAWST output (the simulations without wind turbines) and buoy measurements. The magnitude and time (in UTC) of the maximum wind speed (WS), maximum significant wave height (Hs), and minimum SLP are given for each buoy and simulations with WRF and COAWST (simulated WS at two heights, 10 m | 2.6 m). All the times with Irene are in August 2011. With the simulations, magnitudes are provided every 10 min. With the buoys, magnitudes are provided every 10 min for WS and provided at 50 min past the top of the hour for Hs and SLP.

350

Irene		max WS (m s ⁻¹)	time max WS	max Hs (m)	time max Hs	min SLP (hPa)	time min SLP
41001	buoy	19.7	1840 & 1850 27 Aug	10.0	1550 27 Aug	997.5	1850 27 Aug
	WRF	18.3 16.0	0150 28 Aug	-	-	1002.0	1020 28 Aug
	COAWST	20.2 17.9	0540 28 Aug	5.1	0500 28 Aug	1002.1	1040 28 Aug
41036	buoy	25.1	1620 27 Aug	8.6	0550 27 Aug	957.1	0950 27 Aug
	WRF	27.1 22.9	2240 27 Aug	-	-	965.3	2340 27 Aug
	COAWST	34.4 31.1	2340 27 Aug	7.6	2040 27 Aug	958.2	2210 27 Aug
44007	buoy	16.5	1930 28 Aug	4.5	2150 28 Aug	983.2	0150 29 Aug
	WRF	22.5 15.6	0700 29 Aug	-	-	977.5	0810 29 Aug
	COAWST	23.3 19.1	1140 1150 29 Aug	5.5	0700 29 Aug	975.6	0810 29 Aug
44008	buoy	18.3	1750 28 Aug	8.2	1750 28 Aug	996.1	1950 28 Aug
	WRF	20.0 14.1	0700 29 Aug	-	-	997.7	0420 29 Aug
	COAWST	22.0 15.1	0550 0250 29 Aug	7.9	0650 29 Aug	997.1	0300 29 Aug
44009	buoy	21.4	2140 27 Aug	6.4	0450 28 Aug	958.3	0650 28 Aug
	WRF	27.9 22.1	1330 1710 28 Aug	-	-	974.0	1700 28 Aug
	COAWST	28.6 23.3	1330 1400 28 Aug	6.9	1410 28 Aug	976.5	1610 28 Aug
44013	buoy	18.8	1830 28 Aug	3.8	1550 28 Aug	984.0	2050 28 Aug
	WRF	24.7 17.1	0500 29 Aug	-	-	979.2	0540 29 Aug
	COAWST	22.7 15.7	0410 29 Aug	3.5	0420 & 0430 29 Aug	978.3	0610 29 Aug
44020	buoy	21.2	2350 28 Aug	2.4	1550 28 Aug	989.2	2050 28 Aug
	WRF	26.7 18.5	0600 0840 29 Aug	-	-	987.2	0600 29 Aug
	COAWST	28.0 18.9	0520 29 Aug	3.6	0410 29 Aug	985.9	0520 29 Aug
44065	buoy	21.1	1220 28 Aug	8.0	1250 28 Aug	968.0	1250 28 Aug
	WRF	26.6 19.7	2030 28 Aug 0310 29 Aug	-	-	974.9	2350 28 Aug
	COAWST	27.7 23.9	0350 29 Aug	5.5	2110 28 Aug	973.7	2240 28 Aug



355

Figure 4: Time series of (a, b) wind speeds and wind gusts (WS or WG [$m s^{-1}$]), (c, d) sea surface temperatures (SST [K]), and (e, f) sea level pressure (SLP [hPa]) and significant wave height (Hs [m]) from observations and simulations (WRF and COAWST) for Hurricane Irene (a, c, and e) and Hurricane Sandy (b, d, and f) at buoy 44009 (see location in Fig. 2a). Simulations performed without the action of wind turbines.

360

365

370

375

380



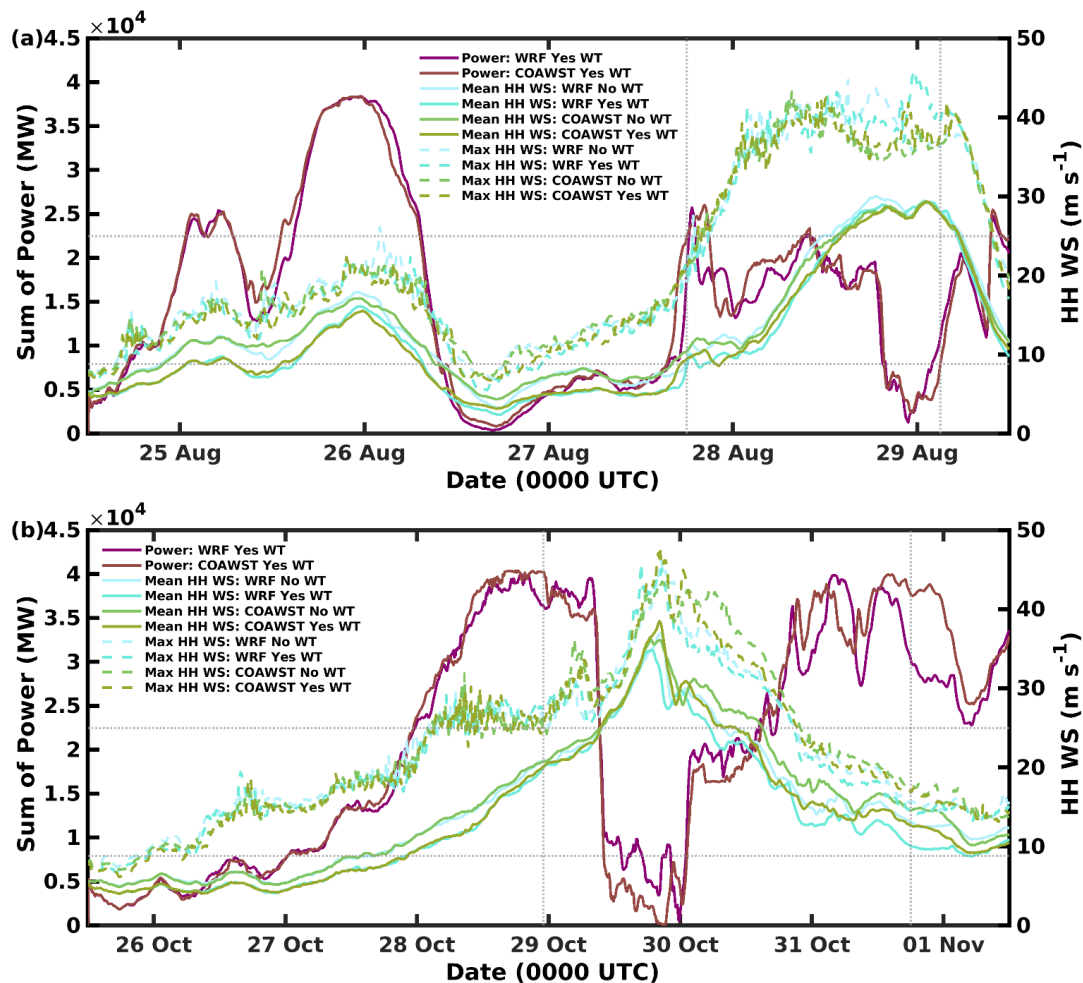
385 **Table 6: Comparison of WRF and COAWST output (the simulations without wind turbines) and buoy measurements. The magnitude and time (in UTC) of the maximum wind speed (WS), maximum significant wave height (Hs), and minimum SLP are given for each buoy and simulations with WRF and COAWST (simulated WS at two heights, 10 m | 2.6 m). All the times with Sandy are in October 2012. With the simulations, magnitudes are provided every 10 min. With the buoys, magnitudes are provided every 10 min for WS and provided at 50 min past the top of the hour for Hs and SLP.**

Sandy		max WS (m s ⁻¹)	time max WS	max Hs (m)	time max Hs	min SLP (hPa)	time min SLP
41001	buoy	28.4	0610 29 Oct	10.1	1350 29 Oct	969.6	2350 28 Oct
	WRF	37.4 32.2	0630 29 Oct	-	-	962.8	0250 29 Oct
	COAWST	36.2 31.8	0630 29 Oct	9.8	1520 28 Oct	964.3	0200 29 Oct
41036	buoy	21.7	2250 27 Oct	5.7	2050 & 2150 27 Oct	992.1	0950 28 Oct
	WRF	25.0 20.9	0720 28 Oct	-	-	995.3	1300 28 Oct
	COAWST	24.6 21.5	0800 28 Oct	5.1	0630 28 Oct	995.0	1530 28 Oct
44007	buoy	18.0	0050 30 Oct	7.1	0350 30 Oct	995.9	0050 30 Oct
	WRF	23.8 16.6	0150 30 Oct	-	-	995.6	0140 30 Oct
	COAWST	23.6 16.6	0020 30 Oct 2350 29 Oct	6.6	0230 30 Oct	995.6	0330 30 Oct
44008	buoy	22.4	1640 29 Oct	11.0	2050 29 Oct	981.2	1750 29 Oct
	WRF	27.4 18.6	1930 29 Oct	-	-	981.9	1830 29 Oct
	COAWST	26.5 21.5	1700 1620 29 Oct	8.6	1750 & 1800 29 Oct	982.5	1810 29 Oct
44009	buoy	23.7	2040 29 Oct	7.4	1050 29 Oct	956.4	2050 29 Oct
	WRF	26.8 22.8	2320 29 Oct 0400 30 Oct	-	-	963.0	0030 30 Oct
	COAWST	29.8 25.6	0210 30 Oct	5.7	2140 29 Oct	950.3	0010 30 Oct
44013	buoy	20.4	1920 29 Oct	6.9	0150 30 Oct	988.2	0050 30 Oct
	WRF	25.0 17.3	2030 29 Oct	-	-	989.2	2300 29 Oct
	COAWST	24.3 16.3	2140 29 Oct	7.0	2210 29 Oct	989.0	2230 29 Oct
44020	buoy	20.6	2000 29 Oct	3.1	1850 29 Oct	983.3	1950 29 Oct
	WRF	28.0 19.0	1940 29 Oct	-	-	984.4	2040 29 Oct
	COAWST	25.9 17.4	1930 29 Oct	2.9	1530 29 Oct	984.7	2110 29 Oct
44065	buoy	24.9	0010 30 Oct	9.9	0050 30 Oct	958.1	2150 29 Oct
	WRF	30.5 22.6	2310 29 Oct 0310 30 Oct	-	-	952.5	2310 29 Oct
	COAWST	30.9 22.7	2200 29 Oct 0100 30 Oct	6.2	0100 30 Oct	960.9	2320 29 Oct

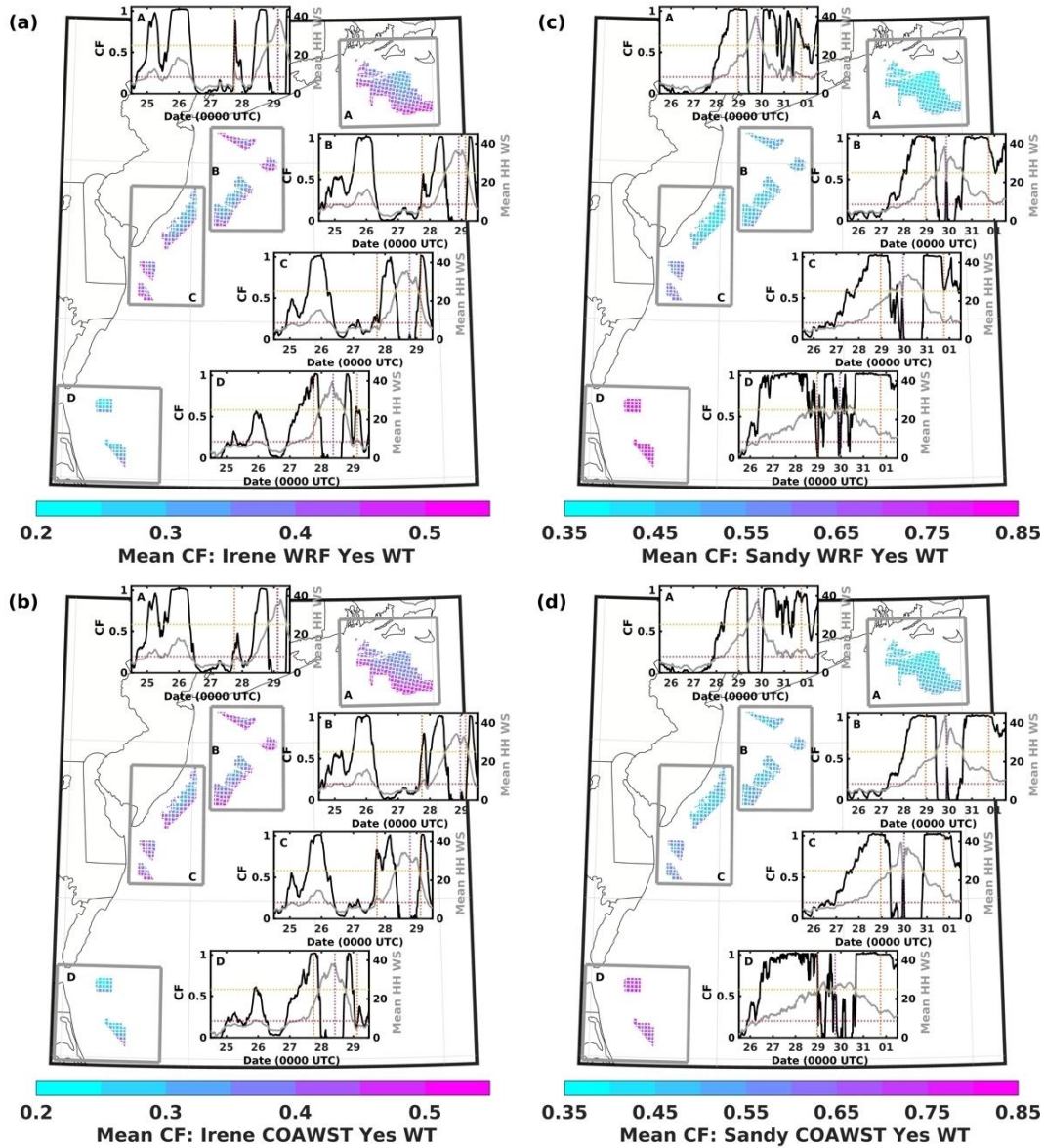
The evaluation of the WRF and COAWST simulations of Hurricane Sandy thus indicates relatively high fidelity. Nevertheless, the fidelity is lower for simulations of Hurricane Irene and biases relative to observations provide important context for the following analyses which focus on power production and extreme conditions at prospective offshore wind turbine locations. Due to the presence of errors in tropical cyclone tracking in the simulations, in the following discussion of geophysical conditions we consider not only grid cells with wind turbines in the LA, but also ocean-based grid cells nearby.

3.2 Wind turbine power production and operating conditions: Hurricane Irene

395 Mean power production and CF computed for the entire Hurricane Irene simulation period using WRF and COAWST are; 1.51×10^4 MW (0.38) and 1.56×10^4 MW (0.39), respectively. When Hurricane Irene is present in d02, equivalent CF are 0.39 and 0.40, respectively. These CF are slightly lower than the climatologically representative estimates of 0.45 presented previously (Pryor and Barthelmie, 2024b, a) due to relatively low wind speeds in the vicinity of the offshore LA early in the simulation and to an extended period of above cut-out wind speeds during the hurricane passage from late on 27 August to the middle of 29 August (Fig. 5a and Fig. 6a, b). However, the system-wide CF only drops below 0.2 for continuous periods of 5 h 50 min (2000 UTC 28 August through 0150 UTC 29 August) in WRF and 7 h 10 min (1950 UTC 28 August through 0300 UTC 29 August) in COAWST (Fig. 5a). At no point is the projected power production zero.



405 Figure 5: Time series of total instantaneous power production from all 2642 wind turbines (left axis) and mean and maximum hub-height wind speed (HH WS, right axis) in grid cells containing wind turbines for (a) Hurricane Irene and (b) Hurricane Sandy simulations. The dashed gray vertical lines mark the start and end time of storm tracking within d02. The lower dashed gray horizontal line marks power production equivalent to a capacity factor of 0.2, and the upper dashed gray horizontal line marks HH WS = 25 m s⁻¹.



410

Figure 6: Mean wind turbine capacity factor (CF) from (a, c) WRF simulations and (b, d) COAWST simulations for (a, b) Hurricane Irene and (c, d) Hurricane Sandy. Also shown are time series of the CF and mean hub-height wind speed (HH WS) for the four LA clusters. Orange dashed lines indicate the start and end time of storm tracking within d02. The purple dashed line represents the time when the location of the minimum SLP is closest to the cluster center. The red dashed line indicates CF = 0.2, yellow line indicates HH WS of 25 m s⁻¹.

415

Time series of power production from WRF and COAWST indicate a high degree of agreement (Fig. 5a) but there are times when the models deviate both in terms of power production and extreme wind speed. Late on 27 August and early on 28 August when Hurricane Irene is south of the LAs, projected power production differs by a maximum of 1.09×10^4 MW (CF difference of 0.275). With WRF, for the 5 h 50 min when the system-wide CF remains below 0.2, the mean HH WS in WT grid cells for the simulation with the WFP active ranges from 27.6 to 29.3 m s⁻¹. Within the LA the maximum HH WS is 45.4 m s⁻¹, which exceeds the 50-year RP WS at 100 m derived in earlier work using ERA5 output (Barthelme et al., 2021),

420



but remains below the 50 m s^{-1} sustained wind speed threshold for class I wind turbines and the 57 m s^{-1} threshold for tropical cyclone hardened wind turbines (class T) (IEC, 2019a). Analyses including all ocean-based grid cells within the four LA clusters indicate the mean HH WS as simulated by WRF with WFP active ranges from 24.2 to 27.0 m s^{-1} and the maximum HH WS reaches 46.4 m s^{-1} . During the period when the system-wide CF from COAWST is < 0.2 , the mean HH WS in WT grid cells ranges from 27.2 to 29.3 m s^{-1} and the maximum reaches 41.8 m s^{-1} . For all ocean-based grid cells within the four LA clusters, the mean HH WS as simulated by COAWST with the WFP active ranges from 23.1 to 27.0 m s^{-1} and the maximum reaches 42.1 m s^{-1} .

430

Mean HH WS $> 25 \text{ m s}^{-1}$ in WT grid cells and CF < 0.2 extend for 13.8, 13.3, and 7.2 h in the WRF simulation with the WFP active and 15.2, 12.8, and 7.3 h in the equivalent simulation with COAWST for LA clusters C, B, and A, respectively (Figs. 6 and 7). Due to slight differences in the hurricane tracking (Fig. 1a), the mean CF from COAWST exceeds that with WRF for offshore LA cluster B and in the northern part of LA cluster C, while the mean CF with WRF exceeds that with COAWST in the southern part of LA cluster C (Fig. 6a, b and Fig. S11). Hurricane Irene tracks very close to LA cluster D, which experiences mean HH WS in WT grid cells $> 25 \text{ m s}^{-1}$ and CF < 0.2 for 15.5 and 17.3 h in the WRF and COAWST simulations, respectively. According to Mood's test, the median CF for this LA from the WRF and COAWST simulations differ at the 95% confidence level.

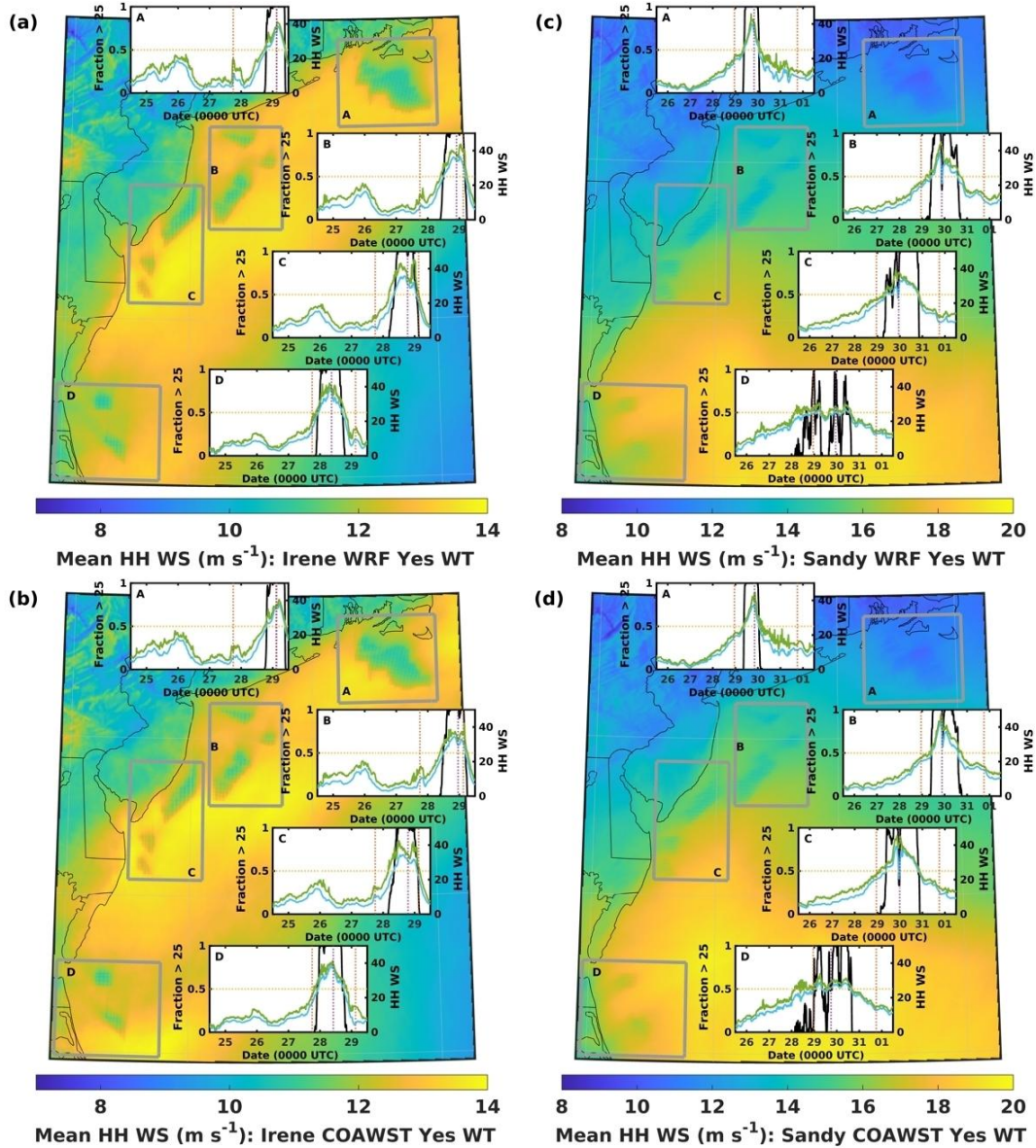
440

Nearly two-thirds of WT-containing grid cells and over three-quarters of ocean grid cells within the LA exhibit a higher frequency of HH WS $> 25 \text{ m s}^{-1}$ in the COAWST simulations when Hurricane Irene is within d02. A larger R_{18} value is also much more frequent ($\geq 96\%$ of time stamps) in each COAWST simulation. Thus, consistent with the analyses of precipitation volume from Hurricane Irene given above, there is evidence that the simulations with COAWST result in a more intense and larger tropical cyclone.

445

In the COAWST simulation with the WFP active, maximum Hs in WT grid cells within LA clusters A, B, C, and D is; 8.6, 8.5, 7.6, and 7.2 m, respectively (Fig. 8), and thus are all below the 50-year RP Hs of $\sim 11 \text{ m}$ estimated using the ERA5 dataset (Barthelmie et al., 2021). LA cluster A exhibits the highest frequency ($\sim 4\%$) of joint Hs, HH WS, and T_p values (Fig. 8) that fall in the classes centered at Hs $\geq 8.4 \text{ m}$, HH WS $\geq 35 \text{ m s}^{-1}$ (approximately equivalent to 5-m WS of 21.5 m s^{-1}), and $T_p \geq 11.2 \text{ s}$ that were previously reported to be associated with high mudline bending moments based on simulations with 3D IFORM applied to the 5 MW NREL offshore reference wind turbine (Valamanesh et al., 2015). The COAWST simulation also indicates frequent occurrence of wind-wave misalignment. In the HH WS class $10.6 - 25 \text{ m s}^{-1}$, 47, 86, 74, and 32% of the time periods have wind-wave misalignment $\geq 30^\circ$ at the center of LA clusters A, B, C, and D, respectively. For HH WS $> 25 \text{ m s}^{-1}$, the corresponding values are 22, 41, 44, and 31%, respectively.

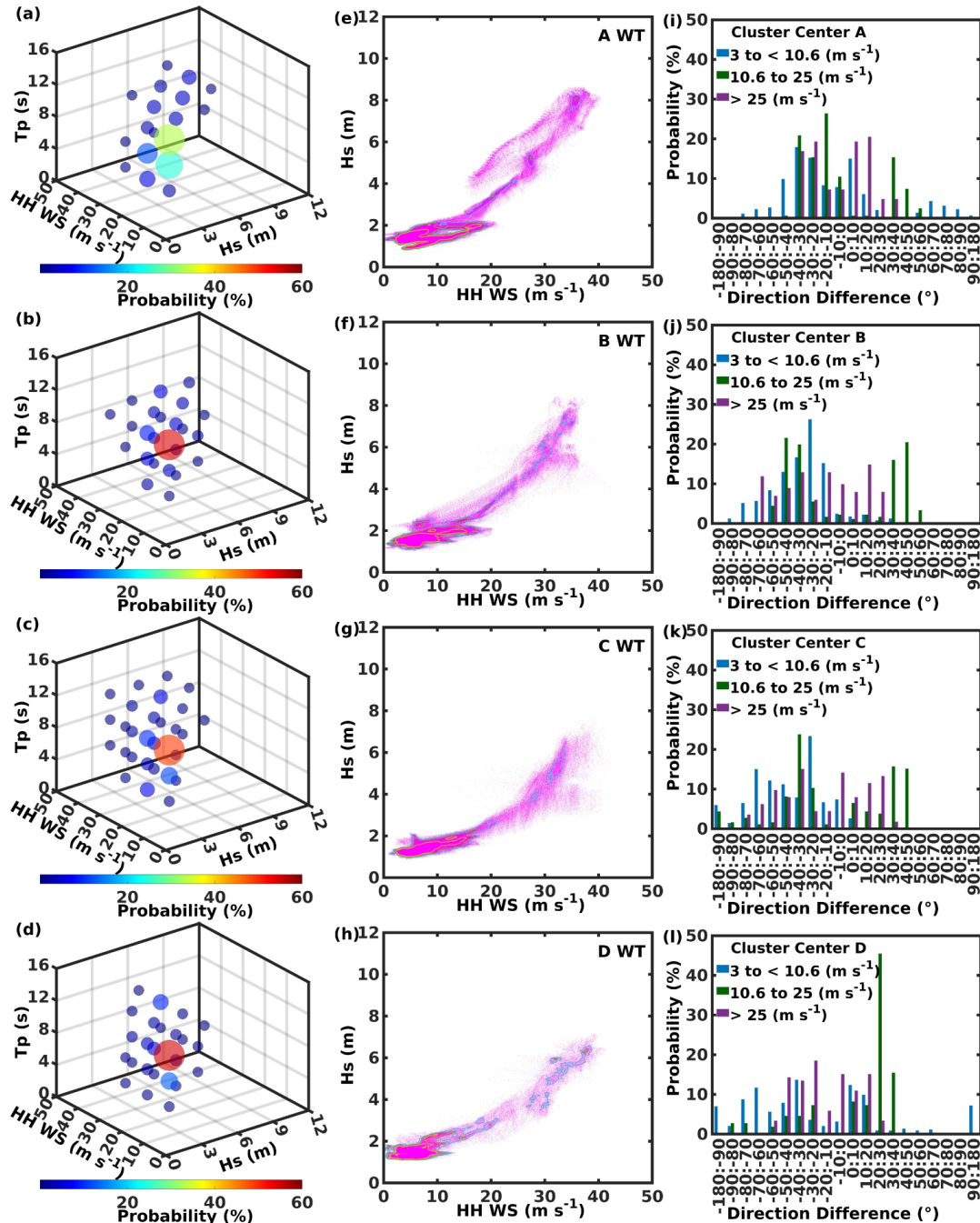
455



460 Figure 7: Mean hub height wind speed (HH WS) and time series of the fraction of wind turbine grid cells with HH WS > 25 m^s⁻¹ (left axis) plus the mean (blue) and maximum (green) HH WS in those grid cells (right axis) in WRF and COAWST simulations with the WFP active. Orange dashed lines indicate the start and end time of storm tracking within d02. The purple dashed line represents the time when the location of the minimum SLP is closest to the cluster center. The yellow line indicates HH WS of 25 m^s⁻¹. For simulations without the WFP active, see Fig. S10.

465

470



475 Figure 8: Extreme conditions based on simulations of Hurricane Irene using COAWST with the WFP active. (a-d) 3-D bubble charts of the joint occurrence of HH WS, Hs, and Tp (5 classes for each variable for a total of 125 possible classes) for all wind turbine grid cells in each LA cluster (A-D). (e-h) Joint probability distributions of HH WS and Hs where the magenta symbols denote 10-min output from all WT grid cells in each LA cluster and the contours denote probability of 0.01 (blue), 0.02 (green), and 0.05 (yellow). (i-l) Histograms of the direction difference (HH WS minus Hs) at the center of each LA cluster for the three HH WS classes: 3 to < 10.6 m s⁻¹, 10.6 to 25 m s⁻¹, and > 25 m s⁻¹.



3.3 Wind turbine power production and operating conditions: Hurricane Sandy

Mean instantaneous power production and CF from WRF and COAWST for the entire Hurricane Sandy simulation period are; 2.03×10^4 MW (0.51) and 2.07×10^4 MW (0.52), respectively. Considering only the time when Hurricane Sandy is within d02, equivalent CF are 0.62 and 0.61, respectively. The high CF are reflective of high, but below cut-out, HH WS prior to the passage of the hurricane over the LA and the relatively short duration of HH WS $> 25 \text{ m s}^{-1}$ within the LA (Fig. 5b and Fig. 6c, d). Simulated system-wide CF drops below 0.2 for 8 h (scattered during 1320 UTC 29 October through 0100 UTC 30 October) in the WRF simulation and for 15 h (1010 UTC 29 October through 0110 UTC 30 October) in the COAWST simulation (Fig. 5b). A single time-step (2100 UTC 29 October) has zero system-wide power production in the COAWST simulation.

490

During periods when the system-wide CF < 0.2 (including landfall in New Jersey), the mean HH WS in WT grid cells is $> 25 \text{ m s}^{-1}$ in both the WRF and COAWST simulations with the WFP active (Fig. 5b). In the WRF simulation with the WFP active, during the longest continuous time when the system-wide CF remains below 0.2 (1710 through 2040 UTC 29 October), the mean HH WS is 30.6 to 34.8 m s^{-1} in WT grid cells and 29.7 to 31.9 m s^{-1} in all ocean-based grid cells within the LA clusters. Equivalent values from COAWST (with WFP active), are 26.0 to 38.5 m s^{-1} and 25.8 to 35.0 m s^{-1} .

495

HH WS $> 50 \text{ m s}^{-1}$ is simulated in tens of thousands of space-time sample combinations in both the WRF and COAWST simulations with the WFP active. However, none occurred within 170 km of any LA centroid. Maximum HH WS in WT grid cells and the frequency of HH WS $> 25 \text{ m s}^{-1}$ in WT grid cells is higher (59% and 65% of time stamps when Hurricane Sandy is within d02) in the COAWST simulation than in the WRF simulation with and without the WFP active (Fig. 7). In all ocean-based grid cells within the LA clusters, 63% and 69% of the time stamps exhibit more grid cells with HH WS $> 25 \text{ m s}^{-1}$ in the COAWST simulations. Maximum HH WS in ocean-based grid cells within the LA clusters is 45.1 m s^{-1} in WRF and 48.9 m s^{-1} in COAWST (Fig. 7). In the COAWST simulation with the WFP active, the maximum HH WS in WT grid cells in LA clusters A, B, and C are; 44.6 , 47.7 , and 45.4 m s^{-1} , respectively (Fig. 9). They thus exceed the highest 50-year RP wind speed at 100 m a.s.l. of 39.7 m s^{-1} computed using ERA5 output (Barthelmie et al., 2021), but are below the 50 m s^{-1} and 57 m s^{-1} thresholds for class I and class T wind turbines (IEC, 2019a). Larger R_{18} values prior to landfall are also more frequent in the COAWST simulations ($> 70\%$ of time stamps in both the simulations without and with the WFP). Thus, consistent with analyses of the simulations of Hurricane Irene, there is evidence that use of COAWST (for the configuration used herein) results in a larger and more intense hurricane.

500

505

510

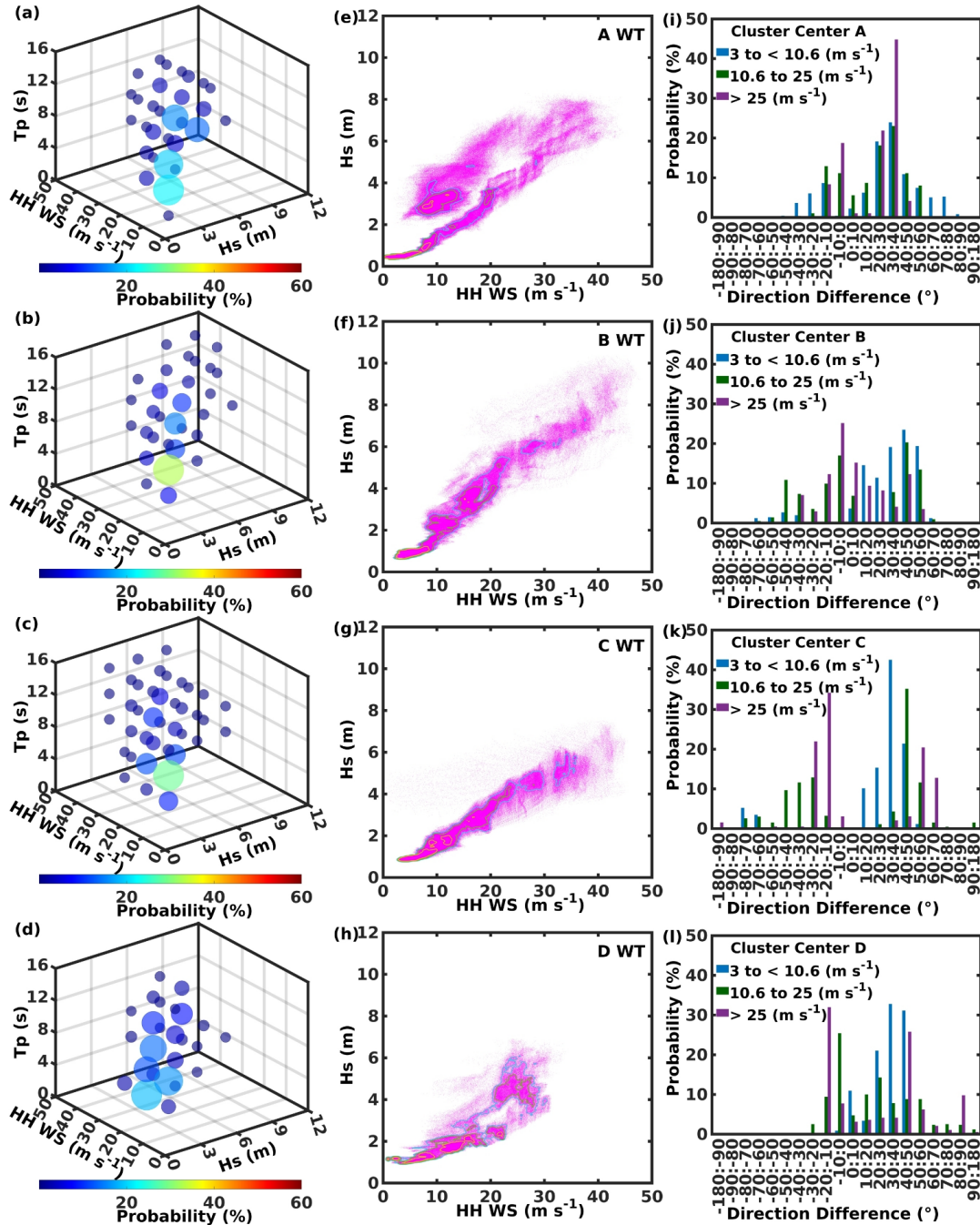
Minor differences in the tracking (Fig. 1b) and intensity of the hurricane-induced wind speeds (Fig. 7), causes higher mean CF from LA cluster A and parts of B and C in the simulation with COAWST than the simulation with WRF (Fig. 6 and Fig. S11). The simulations track the centroid of Hurricane Sandy close to LA clusters B and C and accordingly, periods with CF < 0.2 are of greatest duration for these clusters (20.0 and 23.5 h in WRF and 23.3 and 31.0 h in COAWST, respectively) (Fig. 6). Largest differences in CF are found for LA cluster D. The duration of time with CF < 0.2 is substantially longer in the COAWST simulation due to the prevalence of HH WS $> 25 \text{ m s}^{-1}$ and the median CF for this cluster between the two simulations differs at the 99% confidence level according to Mood's test.

515

Maximum Hs of 8.3, 10.4, 7.5, and 6.9 m in LA clusters A, B, C, and D are higher than those for Hurricane Irene but are also below the 50-year RP values of $\sim 11 \text{ m}$ derived from ERA5 (Barthelmie et al., 2021) (Fig. 9). LA cluster B exhibits the highest frequency ($\sim 4\%$) of joint Hs, HH WS, and Tp values (classes centered at Hs $\geq 8.4 \text{ m}$, HH WS $\geq 35 \text{ m s}^{-1}$ [5-m WS $\sim 21.5 \text{ m s}^{-1}$], and Tp $\geq 11.2 \text{ s}$) close to those associated with a peak mudline moment (of $\sim 120 \text{ MN-m}$) (Valamanesh et al.,

520

2015). Misalignment of wind and waves by $\geq 30^\circ$ is common for both the HH WS class of $10.6 - 25 \text{ m s}^{-1}$ and $> 25 \text{ m s}^{-1}$. Based on COAWST output from the centroids of LA A, B, C, and D, wind-wave misalignment $\geq 30^\circ$ is found for; 43 (49), 525 63 (27), 83 (41) and 34 (49) % of time steps (value in brackets for WS HH $> 25 \text{ m s}^{-1}$).



530 Figure 9: Extreme conditions based on simulations of Hurricane Sandy using COAWST with the WFP active. (a-d) 3-D bubble charts of the joint occurrence of HH WS, Hs, and Tp (5 classes for each variable for a total of 125 possible classes) for all wind turbine grid cells in each LA cluster (A-D). (e-h) Joint probability distributions of HH WS and Hs where the magenta symbols denote 10-min output from all WT grid cells in each LA cluster and the contours denote probability of 0.01 (blue), 0.02 (green), and 0.05 (yellow). (i-l) Histograms of the direction difference (HH WS minus Hs) at the center of each LA cluster for the three HH WS classes: 3 to $< 10.6 \text{ m s}^{-1}$, 10.6 to 25 m s^{-1} , and $> 25 \text{ m s}^{-1}$.

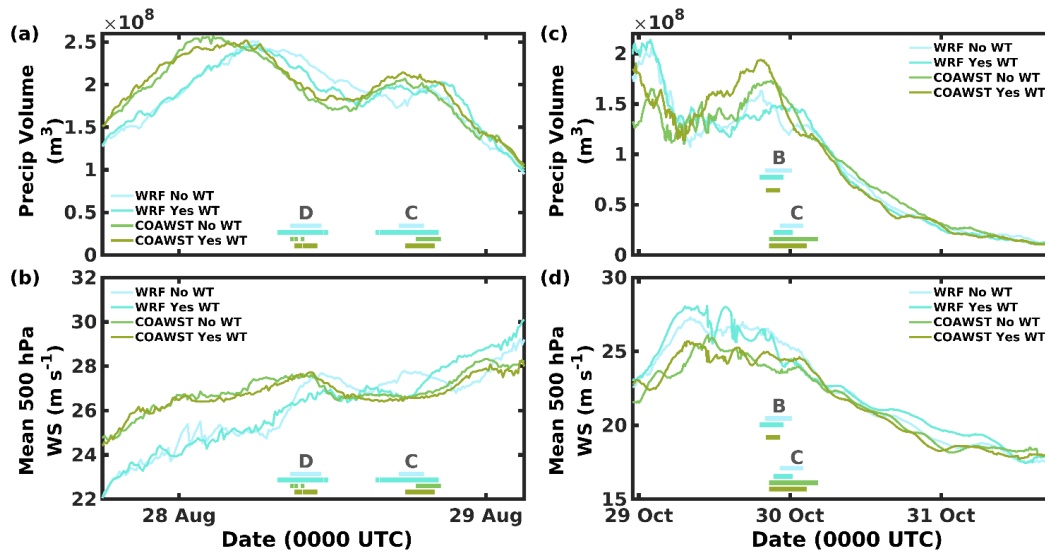


3.4 Wind turbine impacts on hurricane properties

535 Consistent with expectations, removal of kinetic energy by wind turbines means that maximum HH WS in WRF and
COAWST simulations with the WFP active tend to be lower than those when the wind turbines are excluded (see Fig. 5).
For example, output from the no wind turbine COAWST simulation of Hurricane Irene indicates HH WS in ocean-based
grid cells beyond the LA $> 50 \text{ m s}^{-1}$ 837 times while the corresponding number for the simulation with wind turbines is 333.
However, simulations using both WRF and COAWST with full deployment of wind turbines in existing lease areas
540 (approximately 2600 at an ICD of 4.3 MW km^{-2}), indicate that for this scale of offshore wind turbine deployment, the net
impact is small expect for hub-height wind speeds near the lease areas.

For all other metrics, the simulations with WRF or COAWST differ more than the simulations with or without the action of
wind turbines included (Fig. 10). The 10-min mean precipitation volume within 375 km of the Hurricane Irene centroid
545 differs (without WT versus with WFP active) by 4.7% and 3.9% in simulations with WRF and COAWST, respectively, but
differs (WRF versus COAWST) by 11.8% and 9.2% in the no WT and WT simulations, respectively. The equivalent values
for Hurricane Sandy are 8.7% for WRF and 12.9% for COAWST (without WFP active versus with WFP active) and 13.0%
for the no WT and 11.6% for the WT simulations (WRF versus COAWST). Similarly, the mean 500 hPa wind speed close to
the hurricane centroids differ by $< 2 \text{ m s}^{-1}$ in simulations of Hurricanes Irene and Sandy with and without WT with no
550 consistent signal in terms of which simulation is higher (Fig. 10). The mean R_{18} for Hurricane Irene based on WRF
simulations with and without the WFP active differ by $< 2 \text{ km}$ (mean of $\sim 280 \text{ km}$). Mean R_{18} from COAWST simulations
with and without the WFP active also differ by $< 2 \text{ km}$ (mean of $\sim 300 \text{ km}$). Thus, while median R_{18} from WRF versus
COAWST are statistically different (at $p < 0.01$) for simulations with and without the WFP active, the use of the WFP does
not yield significantly different R_{18} values in simulations with a given model. Simulations with WFP active produce equal or
555 slightly more total precipitation. For Hurricane Irene, the 10-min mean (median) precipitation volume from WRF without
and with the WFP active are $1.88 \times 10^8 \text{ m}^3$ ($1.89 \times 10^8 \text{ m}^3$) and $1.88 \times 10^8 \text{ m}^3$ ($1.93 \times 10^8 \text{ m}^3$), while equivalent values from
COAWST are $1.93 \times 10^8 \text{ m}^3$ ($1.93 \times 10^8 \text{ m}^3$) and $1.98 \times 10^8 \text{ m}^3$ ($2.02 \times 10^8 \text{ m}^3$), respectively. For Hurricane Sandy, the
corresponding values are $8.64 \times 10^7 \text{ m}^3$ ($8.60 \times 10^7 \text{ m}^3$) versus $8.68 \times 10^7 \text{ m}^3$ ($8.10 \times 10^7 \text{ m}^3$) from WRF and $8.69 \times 10^7 \text{ m}^3$
($9.19 \times 10^7 \text{ m}^3$) versus $8.87 \times 10^7 \text{ m}^3$ ($7.79 \times 10^7 \text{ m}^3$) from COAWST.

560



565 Figure 10: Time series of (a, c) 10-min precipitation volume within a 375 km radius from the minimum SLP location and (b, d)
 570 mean 500 hPa wind speed of grid cells from 50 to 375 km from the minimum SLP location in d02 for simulations with WRF and
 COAWST of (a, b) Hurricane Irene and (c, d) Hurricane Sandy. The horizontal lines near “D” and “C” in panels a and b and near
 “B” and “C” for panels c and d, mark the times when the minimum SLP is within 100 km of the center of the specified offshore
 wind energy LA cluster. See Fig. S12 for comparison of wind speeds at 10-m a.s.l.

570 4 Concluding remarks

Results of analyses of simulations with WRF and COAWST of two of the most powerful hurricanes that tracked within 100
 km of offshore wind energy lease areas along the U.S. East Coast during the last 25 years can be summarized as:

- 1) Many aspects of Hurricane Sandy are well reproduced in WRF and COAWST control simulations that exclude the
 575 action of wind turbines. Consistent with past research, simulations of Hurricane Irene exhibit lower fidelity relative
 to a range of observations in part due to the negative bias in translational speed. In contrast to similar simulations of
 Typhoon Muifa (Liu et al., 2015) but consistent with past research on intense cyclones in the North Sea (Larsén et
 al., 2019), COAWST simulations of both hurricanes indicate a slightly larger area of storm-force wind speeds (R_{18})
 and hub-height wind speeds $> 25 \text{ m s}^{-1}$ plus higher precipitation volumes than are indicated by the WRF
 580 simulations. This coupled with the ability of COAWST to quantify additional geophysical parameters of importance
 to offshore structures strongly indicates the need for increasing investment in coupled simulations for the offshore
 wind energy industry.
- 2) Despite the intensity and size of these hurricanes and their proximity to the offshore wind energy lease areas,
 585 simulations presented herein, that assume a 15 MW reference wind turbine deployed with a spacing of 1.85 km,
 indicate only fairly brief periods with low power production (system-wide CF < 0.2). System-wide capacity factors
 below 0.2 due to wide-spread occurrence of hub-height wind speeds above 25 m s^{-1} extend for only 6-7 h in the
 simulations of Hurricane Irene and 8-15 h for Hurricane Sandy (the longer period is based on the simulation with
 COAWST). Further, neither hurricane is simulated to produce hub-height wind speeds $> 50 \text{ m s}^{-1}$ in the current
 590 offshore lease areas. Thus, based on these simulations of these intense tropical cyclones there is no evidence of a
 need for hurricane hardening of wind turbines deployed in the current offshore lease areas. Also, these simulations
 suggest even such that the projected fleet of offshore wind turbines will continue to supply substantial amounts of



electricity to the grid even during these extreme events. However, simulations of both hurricanes with COAWST result in wave-wind conditions that have previously been identified as being associated with high mudline bending moments on monopile foundations. The COAWST simulations of both hurricanes also indicate a relative high frequency of HH WS-wave directional misalignment ($> 30^\circ$) in these lease areas.

3) There is no evidence that deployment of 2642 wind turbines at an ICD of 4.3 MW km^{-2} within existing offshore wind energy lease areas along the U.S. East Coast would have substantially weakened either of the hurricanes considered herein. Although much denser and larger deployments might have an influence on hurricanes, even for Hurricane Irene that tracked closest to the offshore wind energy lease areas, simulations with either WRF or COAWST differ more than simulations with either WFP inactive or active with respect to the volume of precipitation near the hurricane center, storm intensity, and/or extent.

Mesoscale simulations performed at convection permitting resolution such as those presented herein allow simulation of the hurricane lifespans and associated power production over large domains and can be used as here to assess whether improved treatment of atmosphere-ocean dynamical coupling alters extreme conditions of relevance to offshore wind turbines. However, it is important to acknowledge that the highest structural loading may occur in the cyclone eye-wall (Han et al., 2014) that is of a scale (Marks et al., 2008) that is not fully represented in the simulations presented here. Nevertheless, analyses of the simulations suggest the structure of the hurricanes is reasonably represented in our modeling (Fig. 3) and simulations performed at the same grid spacing were shown to represent some aspects of flow in the eye wall (Müller et al., 2024). Future work employing mesoscale-microscale coupling (Wang et al., 2024) could be used to evolve further details of geophysical properties of relevance to structural loading. Further, the hurricanes simulated herein were extremely powerful and both tracked within 100 km of offshore wind energy lease area cluster centers (C and D for Hurricane Irene, B and C for Hurricane Sandy). However, they do not represent a comprehensive climatology of historical or possible intense tropical/extratropical cyclones (Barthelmie et al., 2021). Undertaking comparable simulations of additional extreme cyclones would also be useful in determining if findings presented herein are generalizable and to quantify the degree to which the meteorological and oceanic extreme conditions vary according to the precise model formulation.

Code and data availability

COAWST software can be downloaded from: <https://github.com/DOI-USGS/COAWST>. NAM data can be downloaded from: <https://rda.ucar.edu/datasets/d609000/> and <https://www.ncei.noaa.gov/products/weather-climate-models/north-american-mesoscale>. OSTIA-UKMO-L4-GLOB-v2.0 SST data can be downloaded from: <https://podaac.jpl.nasa.gov/dataset/OSTIA-UKMO-L4-GLOB-v2.0>. GHSHHG data can be downloaded from: <https://www.ngdc.noaa.gov/mgg/shorelines/>. GEBCO data can be downloaded from: <https://download.gebco.net/>. HYCOM GLBa0.08 expt 90.9 data can be downloaded from: <https://tds.hycom.org/thredds/catalog.html>. ADCIRC 2001v2d data can be downloaded from: <https://adcirc.org/products/adcirc-tidal-databases/>. GFS wind forcing data can be downloaded from: <https://www.ncei.noaa.gov/thredds/catalog/model/gfs.html>. WW3 data for boundary conditions can be downloaded from: <https://www.ncei.noaa.gov/thredds-ocean/catalog/ncep/nww3/catalog.html>. NHC “best track” data can be downloaded from: <https://www.nhc.noaa.gov/data/tcr/index.php>. HURDAT2 data can be downloaded from: <https://www.nhc.noaa.gov/data/#hurdat>. IMERG V07 data can be downloaded from: https://disc.gsfc.nasa.gov/datasets/GPM_3IMERGHH_07/summary?keywords=“IMERG_final”. NDBC buoy data can be downloaded from: <https://www.ndbc.noaa.gov/>. Scientific color maps can be downloaded from <https://www.fabiocrameri.ch/colourmaps/> (Crameri et al., 2020).



Supplemental materials

635 See the attached document.

Author contributions

SCP and RJB obtained funding and computing support for this work. KBT performed the simulations, SCP and KBT processed data used for model evaluation, conducted the analyses with assistance from RJB, produced the figures, and drafted the initial manuscript. All authors contributed to the design of the analyses, interpretation of results, and manuscript
640 revisions.

Competing interests

The authors declare that they have no conflict of interest.

Acknowledgements

This research was supported by the Cornell Atkinson Center for Sustainability (AVF-AOWE) and the U.S. Department of
645 Energy Office of Science (DE-SC0016605). Computing resources were provided by NSF Extreme Science and Engineering
Discovery Environment (XSEDE) (award TG-ATM170024) and the National Energy Research Scientific Computing Center,
a DoE Office of Science User Facility supported by the Office of Science of the U.S. Department of Energy under Contract
No. DE-AC02-05CH11231. Any opinions, findings, and conclusions or recommendations expressed in this material are
those of the authors and do not necessarily reflect the views of these agencies. We thank Dr. John Warner for his help in
650 answering COAWST-related questions.

References

- Avila, L. A. and Cangialosi, J.: Tropical Cyclone Report: Hurricane Irene, 45,
https://www.nhc.noaa.gov/data/tcr/AL092011_Irene.pdf, 2011.
- 655 Baldini, L. M., Baldini, J. U. L., McElwaine, J. N., Frappier, A. B., Asmerom, Y., Liu, K.-b., Pruger, K. M., Ridley, H. E.,
Polyak, V., Kennett, D. J., Macpherson, C. G., Aquino, V. V., Awe, J., and Breitenbach, S. F. M.: Persistent northward
North Atlantic tropical cyclone track migration over the past five centuries, *Scientific Reports*, 6, 37522,
<https://www.nature.com/articles/srep37522>, 2016.
- Barthelmie, R. J., Dantuono, K. E., Renner, E. J., Letson, F. L., and Pryor, S. C.: Extreme Wind and Waves in U.S. East
660 Coast Offshore Wind Energy Lease Areas, *Energies*, 14, 1053, <https://www.mdpi.com/1996-1073/14/4/1053>, 2021.
- Blake, E. S., Kimberlain, T. B., Berg, R. J., Cangialosi, J. P., and Beven II, J. L.: Tropical Cyclone Report: Hurricane Sandy,
National Hurricane Center, 157, https://www.nhc.noaa.gov/data/tcr/AL182012_Sandy.pdf, 2013.
- Bodini, N., Optis, M., Redfern, S., Rosencrans, D., Rybchuck, A., Lundquist, J., Pronk, V., Castagneri, S., Purkayastha, A.,
Draxl, C., Krishnamurthy, R., Young, E., Roberts, B., Rosenlieb, E., and Musial, W.: The 2023 National Offshore Wind
665 Data Set (NOW-23), *Earth System Science Data*, 16, 1965-2006, [https://research-hub.nrel.gov/en/publications/the-2023-
national-offshore-wind-data-set-now-23](https://research-hub.nrel.gov/en/publications/the-2023-national-offshore-wind-data-set-now-23), 2024.
- Booij, N., Ris, R. C., and Holthuijsen, L. H.: A third-generation wave model for coastal regions: 1. Model description and
validation, *Journal of Geophysical Research: Oceans*, 104, 7649-7666,
<https://agupubs.onlinelibrary.wiley.com/doi/abs/10.1029/98JC02622>, 1999.
- 670 Calvo-Sancho, C., Quiñán-Hernández, L., González-Alemán, J. J., Bolgiani, P., Santos-Muñoz, D., and Martín, M. L.:
Assessing the performance of the HARMONIE-AROME and WRF-ARW numerical models in North Atlantic Tropical



- Transitions, Atmospheric Research, 291, 106801, <https://www.sciencedirect.com/science/article/pii/S0169809523001989>, 2023.
- 675 Chen, F. and Dudhia, J.: Coupling an Advanced Land Surface–Hydrology Model with the Penn State–NCAR MM5 Modeling System. Part I: Model Implementation and Sensitivity, Monthly Weather Review, 129, 569-585, https://journals.ametsoc.org/view/journals/mwre/129/4/1520-0493_2001_129_0569_caalsh_2.0.co_2.xml, 2001a.
- Chen, F. and Dudhia, J.: Coupling an Advanced Land Surface–Hydrology Model with the Penn State–NCAR MM5 Modeling System. Part II: Preliminary Model Validation, Monthly Weather Review, 129, 587-604, https://journals.ametsoc.org/view/journals/mwre/129/4/1520-0493_2001_129_0587_caalsh_2.0.co_2.xml, 2001b.
- 680 Chen, X. and Xu, J. Z.: Structural failure analysis of wind turbines impacted by super typhoon Usagi, Engineering Failure Analysis, 60, 391-404, <https://www.sciencedirect.com/science/article/pii/S1350630715301552?via%3Dihub>, 2016.
- Chen, Y. and Yau, M. K.: Asymmetric Structures in a Simulated Landfalling Hrrricane, Journal of the Atmospheric Sciences, 60, 2294-2312, https://journals.ametsoc.org/view/journals/atsc/60/18/1520-0469_2003_060_2294_asiasl_2.0.co_2.xml, 2003.
- 685 Crameri, F., Shephard, G. E., and Heron, P. J.: The misuse of colour in science communication, Nature Communications, 11, 5444, <https://www.nature.com/articles/s41467-020-19160-7>, 2020.
- Davis, C., Wang, W., Chen, S. S., Chen, Y., Corbosiero, K., DeMaria, M., Dudhia, J., Holland, G., Klemp, J., Michalakes, J., Reeves, H., Rotunno, R., Snyder, C., and Xiao, Q.: Prediction of Landfalling Hurricanes with the Advanced Hurricane WRF Model, Monthly Weather Review, 136, 1990-2005, <https://journals.ametsoc.org/view/journals/mwre/136/6/2007mwr2085.1.xml>, 2008.
- Drennan, W. M., Taylor, P. K., and Yelland, M. J.: Parameterizing the Sea Surface Roughness, Journal of Physical Oceanography, 35, 835-848, <https://journals.ametsoc.org/view/journals/phoc/35/5/jpo2704.1.xml>, 2005.
- Dudhia, J.: Numerical Study of Convection Observed during the Winter Monsoon Experiment Using a Mesoscale Two-Dimensional Model, Journal of the Atmospheric Sciences, 46, 3077-3107, https://journals.ametsoc.org/view/journals/atsc/46/20/1520-0469_1989_046_3077_nsocod_2_0_co_2.xml, 1989.
- 695 Ek, M. B., Mitchell, K. E., Lin, Y., Rogers, E., Grunmann, P., Koren, V., Gayno, G., and Tarpley, J. D.: Implementation of Noah land surface model advances in the National Centers for Environmental Prediction operational mesoscale Eta model, Journal of Geophysical Research: Atmospheres, 108, 8851, <https://agupubs.onlinelibrary.wiley.com/doi/full/10.1029/2002JD003296>, 2003.
- 700 Fischer, T., Rainey, P., Bossanyi, E., and Kühn, M.: Study on Control Concepts suitable for Mitigation of Loads from Misaligned Wind and Waves on Offshore Wind Turbines supported on Monopiles, Wind Engineering, 35, 561-573, <https://journals.sagepub.com/doi/10.1260/0309-524X.35.5.561>, 2011.
- Fitch, A. C., Olson, J. B., Lundquist, J. K., Dudhia, J., Gupta, A. K., Michalakes, J., and Barstad, I.: Local and Mesoscale Impacts of Wind Farms as Parameterized in a Mesoscale NWP Model, Monthly Weather Review, 140, 3017-3038, <https://journals.ametsoc.org/view/journals/mwre/140/9/mwr-d-11-00352.1.xml>, 2012.
- 705 Foody, R., Coburn, J., Aird, J. A., Barthelmie, R. J., and Pryor, S. C.: Quantitative comparison of power production and power quality onshore and offshore: a case study from the eastern United States, Wind Energy Science, 9, 263-280, <https://wes.copernicus.org/articles/9/263/2024/wes-9-263-2024.pdf>, 2024.
- Gaertner, E., Rinker, J., Sethuraman, L., Zahle, F., Anderson, B., Barter, G., Abbas, N., Meng, F., Bortolotti, P., Skrzypinski, W., Scott, G., Feil, R., Bredmose, H., Dykes, K., Shields, M., Allen, C., and Viselli, A.: IEA Wind TCP Task 37: Definition of the IEA 15-Megawatt Offshore Reference Wind Turbine, National Renewable Energy Lab.(NREL), Golden, CO (United States), 54, <https://www.nrel.gov/docs/fy20osti/75698.pdf>, 2020.
- Gaudet, B. J., García Medina, G., Krishnamurthy, R., Shaw, W. J., Sheridan, L. M., Yang, Z., Newsom, R. K., and Pekour, M.: Evaluation of Coupled Wind–Wave Model Simulations of Offshore Winds in the Mid-Atlantic Bight Using Lidar-Equipped Buoys, Monthly Weather Review, 150, 1377-1395, <https://journals.ametsoc.org/view/journals/mwre/150/6/MWR-D-21-0166.1.xml>, 2022.
- 715 GWEC: Global Wind Report 2024, Global Wind Energy Council, Brussels, Belgium. , 168, <https://gwec.net/global-wind-report-2024/>, 2024a.



- 720 GWEC: Global Offshore Wind Report 2024, Global Wind Energy Council, Brussels, Belgium. , 156, <https://gwec.net/global-offshore-wind-report-2024/> 2024b.
- 725 Haidvogel, D. B., Arango, H., Budgell, W. P., Cornuelle, B. D., Curchitser, E., Di Lorenzo, E., Fennel, K., Geyer, W. R., Hermann, A. J., Lanerolle, L., Levin, J., McWilliams, J. C., Miller, A. J., Moore, A. M., Powell, T. M., Shchepetkin, A. F., Sherwood, C. R., Signell, R. P., Warner, J. C., and Wilkin, J.: Ocean forecasting in terrain-following coordinates: Formulation and skill assessment of the Regional Ocean Modeling System, *Journal of Computational Physics*, 227, 3595-3624, <https://www.sciencedirect.com/science/article/abs/pii/S0021999107002549>, 2008.
- Hallowell, S. T., Myers, A. T., Arwade, S. R., Pang, W., Rawal, P., Hines, E. M., Hajjar, J. F., Qiao, C., Valamanesh, V., Wei, K., Carswell, W., and Fontana, C. M.: Hurricane risk assessment of offshore wind turbines, *Renewable Energy*, 125, 234-249, <https://www.sciencedirect.com/science/article/pii/S0960148118302349>, 2018.
- 730 Han, T., McCann, G., Mücke, T. A., and Freudenreich, K.: How can a wind turbine survive in tropical cyclone?, *Renewable energy*, 70, 3-10, <https://www.sciencedirect.com/science/article/pii/S0960148114000949>, 2014.
- Hansen, T. A., Wilson, E. J., Fitts, J. P., Jansen, M., Beiter, P., Steffen, B., Xu, B., Guillet, J., Münster, M., and Kitzing, L.: Five grand challenges of offshore wind financing in the United States, *Energy Research & Social Science*, 107, 103329, <https://www.sciencedirect.com/science/article/pii/S2214629623003894>, 2024.
- 735 Hashemi, M. R., Kresning, B., Hashemi, J., and Ginis, I.: Assessment of hurricane generated loads on offshore wind farms; a closer look at most extreme historical hurricanes in New England, *Renewable Energy*, 175, 593-609, <https://www.sciencedirect.com/science/article/pii/S0960148121007187>, 2021.
- Hettmansperger, T. P. and Malin, J. S.: A modified Mood's test for location with no shape assumptions on the underlying distributions, *Biometrika*, 62, 527-529, <https://www.jstor.org/stable/2335398?seq=1>, 1975.
- 740 Hong, S.-Y. and Lim, J.-O. J.: The WRF single-moment 6-class microphysics scheme (WSM6), *Journal of the Korean Meteorological Society*, 42, 129-151, https://www.researchgate.net/publication/331192569_Hongandlim-JKMS-2006, 2006.
- Huffman, G. J., Bolvin, D. T., Joyce, R., Kelley, O. A., Nelkin, E. J., Portier, A., Stocker, E. F., Tan, J., Watters, D. C., and West, B. J.: IMERG V07 Release Notes, 17, https://gpm.nasa.gov/sites/default/files/2024-02/IMERG_V07_ReleaseNotes_240221.pdf, 2024.
- 745 IEC: IEC 61400-3-1:2019. Wind energy generation systems. Part 3–1: Design requirements for fixed offshore wind turbines, International Electrotechnical Commission, Geneva, Switzerland. ISBN: 9780580944345, Geneva, Switzerland, 2019a.
- IEC: IEC 61400-1 Edition 4.0 2019-02 Wind turbines – Part 1: Design requirements, International Electrotechnical Commission, Geneva, Switzerland. ISBN 978-2-8322-6253-5, Geneva, Switzerland, 2019b.
- Jacob, R., Larson, J., and Ong, E.: $M \times N$ Communication and Parallel Interpolation in CCSM Using the Model Coupling Toolkit, 33, <https://www.mcs.anl.gov/research/projects/acpi/mct/mxnP1225.pdf>, 2005.
- 750 Jacobson, M. Z., Archer, C. L., and Kempton, W.: Taming hurricanes with arrays of offshore wind turbines, *Nature Climate Change*, 4, 195-200, <https://www.nature.com/articles/nclimate2120>, 2014.
- Jansen, M., Staffell, I., Kitzing, L., Quoilin, S., Wiggelinkhuizen, E., Bulder, B., Riepin, I., and Müsgens, F.: Offshore wind competitiveness in mature markets without subsidy, *Nature Energy*, 5, 614-622, <https://www.nature.com/articles/s41560-020-0661-2>, 2020.
- 755 Ju, S.-H., Hsu, H.-H., and Hsiao, T.-Y.: Three-dimensional wind fields of tropical cyclones for wind turbine structures, *Ocean Engineering*, 237, 109437, <https://www.sciencedirect.com/science/article/pii/S0029801821008428>, 2021.
- Kain, J. S.: The Kain–Fritsch Convective Parameterization: An Update, *Journal of Applied Meteorology*, 43, 170-181, https://journals.ametsoc.org/view/journals/apme/43/1/1520-0450_2004_043_0170_tkcpau_2.0.co_2.xml, 2004.
- 760 Khaira, U. and Astitha, M.: Exploring the Real-Time WRF Forecast Skill for Four Tropical Storms, Isaias, Henri, Elsa and Irene, as They Impacted the Northeast United States, *Remote Sensing*, 15, 3219, <https://www.mdpi.com/2072-4292/15/13/3219>, 2023.
- Koukoura, C., Brown, C., Natarajan, A., and Vesth, A.: Cross-wind fatigue analysis of a full scale offshore wind turbine in the case of wind–wave misalignment, *Engineering Structures*, 120, 147-157, <https://www.sciencedirect.com/science/article/pii/S0141029616301389>, 2016.



- 765 Kresning, B., Hashemi, M. R., and Gallucci, C.: Simulation of Hurricane Loading for Proposed Offshore Windfarms off the US Northeast Coast, *Journal of Physics: Conference Series*, 12 pp, <https://iopscience.iop.org/article/10.1088/1742-6596/1452/1/012026>, 2020.
- Kresning, B., Hashemi, M. R., Shirvani, A., and Hashemi, J.: Uncertainty of extreme wind and wave loads for marine renewable energy farms in hurricane-prone regions, *Renewable Energy*, 220, 119570, <https://www.sciencedirect.com/science/article/pii/S0960148123014854>, 2024.
- 770 Lackmann, G. M.: Hurricane Sandy before 1900 and after 2100, *Bulletin of the American Meteorological Society*, 96, 547-560, <https://journals.ametsoc.org/view/journals/bams/96/4/bams-d-14-00123.1.xml>, 2015.
- Landsea, C. W. and Franklin, J. L.: Atlantic Hurricane Database Uncertainty and Presentation of a New Database Format, *Monthly Weather Review*, 141, 3576-3592, <https://journals.ametsoc.org/view/journals/mwre/141/10/mwr-d-12-00254.1.xml>, 2013.
- 775 Larsén, X. G. and Ott, S.: Adjusted spectral correction method for calculating extreme winds in tropical-cyclone-affected water areas, *Wind Energy Science*, 7, 2457-2468, <https://wes.copernicus.org/articles/7/2457/2022/>, 2022.
- Larsén, X. G., Ott, S., Badger, J., Hahmann, A. N., and Mann, J.: Recipes for Correcting the Impact of Effective Mesoscale Resolution on the Estimation of Extreme Winds, *Journal of Applied Meteorology and Climatology*, 51, 521-533, <https://journals.ametsoc.org/view/journals/apme/51/3/jamc-d-11-090.1.xml>, 2012.
- 780 Larsén, X. G., Du, J., Bolaños, R., Imberger, M., Kelly, M. C., Badger, M., and Larsen, S.: Estimation of offshore extreme wind from wind-wave coupled modeling, *Wind Energy*, 22, 1043-1057, <https://onlinelibrary.wiley.com/doi/epdf/10.1002/we.2339>, 2019.
- Larson, J., Jacob, R., and Ong, E.: The Model Coupling Toolkit: A New Fortran90 Toolkit for Building Multiphysics Parallel Coupled Models, *The International Journal of High Performance Computing Applications*, 19, 277-292, <https://journals.sagepub.com/doi/10.1177/1094342005056115>, 2005.
- 785 Li, J., Li, Z., Jiang, Y., and Tang, Y.: Typhoon Resistance Analysis of Offshore Wind Turbines: A Review, *Atmosphere*, 13, 451, <https://www.mdpi.com/2073-4433/13/3/451>, 2022.
- Li, S. and Chen, C.: Air-sea interaction processes during hurricane Sandy: Coupled WRF-FVCOM model simulations, *Progress in Oceanography*, 206, 102855, <https://www.sciencedirect.com/science/article/pii/S0079661122001148>, 2022.
- 790 Liu, N., Ling, T., Wang, H., Zhang, Y., Gao, Z., and Wang, Y.: Numerical Simulation of Typhoon Muifa (2011) Using a Coupled Ocean-Atmosphere-Wave-Sediment Transport (COAWST) Modeling System, *Journal of Ocean University of China*, 14, 199-209, <https://link.springer.com/article/10.1007/s11802-015-2415-5>, 2015.
- Marks, F. D., Black, P. G., Montgomery, M. T., and Burpee, R. W.: Structure of the Eye and Eyewall of Hurricane Hugo (1989), *Monthly Weather Review*, 136, 1237-1259, <https://journals.ametsoc.org/view/journals/mwre/136/4/2007mwr2073.1.xml>, 2008.
- 795 Martín del Campo, J. O., Pozos-Estrada, A., and Pozos-Estrada, O.: Development of fragility curves of land-based wind turbines with tuned mass dampers under cyclone and seismic loading, *Wind Energy*, 24, 737-753, <https://onlinelibrary.wiley.com/doi/full/10.1002/we.2600>, 2021.
- 800 Marvel, K., Kravitz, B., and Caldeira, K.: Geophysical limits to global wind power, *Nature Climate Change*, 3, 118-121, <https://www.nature.com/articles/nclimate1683>, 2013.
- McElman, S., Verma, A., and Goupee, A.: Quantifying Tropical Cyclone-Generated Waves in Extreme-Value-Derived Design for Offshore Wind, *Wind Energy Science Discussions*, 2024, <https://wes.copernicus.org/preprints/wes-2024-129/>, 2024.
- 805 Mlawer, E. J., Taubman, S. J., Brown, P. D., Iacono, M. J., and Clough, S. A.: Radiative transfer for inhomogeneous atmospheres: RRTM, a validated correlated-k model for the longwave, *Journal of Geophysical Research: Atmospheres*, 102, 16663-16682, <https://agupubs.onlinelibrary.wiley.com/doi/abs/10.1029/97JD00237>, 1997.
- Mooney, P. A., Gill, D. O., Mulligan, F. J., and Bruyère, C. L.: Hurricane simulation using different representations of atmosphere-ocean interaction: the case of Irene (2011), *Atmospheric Science Letters*, 17, 415-421, <https://rmetsonline.wiley.com/doi/10.1002/asl.673>, 2016.
- 810



- Mooney, P. A., Mulligan, F. J., Bruyère, C. L., Parker, C. L., and Gill, D. O.: Investigating the performance of coupled WRF-ROMS simulations of Hurricane Irene (2011) in a regional climate modeling framework, *Atmospheric Research*, 215, 57-74, <https://www.sciencedirect.com/science/article/pii/S0169809517313091>, 2019.
- 815 Morin, G., Boudreault, M., and García-Franco, J. L.: A Global Multi-Source Tropical Cyclone Precipitation (MSTCP) Dataset, *Scientific Data*, 11, 609, <https://www.nature.com/articles/s41597-024-03395-w>, 2024.
- Mudd, L. A. and Vickery, P. J.: Gulf of Mexico Hurricane Risk Assessment for Offshore Wind Energy Sites, *Wind Energy Science Discussions*, 2024, <https://wes.copernicus.org/preprints/wes-2024-123/>, 2024.
- Mukherjee, P. and Ramakrishnan, B.: On the understanding of very severe cyclone storm Ockhi with the WRF-ARW model, *Environmental Research: Climate*, 1, 015002, <https://iopscience.iop.org/article/10.1088/2752-5295/ac6adb>, 2022.
- 820 Müller, S., Larsén, X. G., and Verelst, D. R.: Tropical cyclone low-level wind speed, shear, and veer: sensitivity to the boundary layer parametrization in the Weather Research and Forecasting model, *Wind Energy Science*, 9, 1153-1171, <https://wes.copernicus.org/articles/9/1153/2024/>, 2024.
- Nakanishi, M. and Niino, H.: An Improved Mellor–Yamada Level-3 Model: Its Numerical Stability and Application to a Regional Prediction of Advection Fog, *Boundary-Layer Meteorology*, 119, 397-407, 825 <https://link.springer.com/article/10.1007/s10546-005-9030-8>, 2006.
- NDBC: Handbook of Automated Data Quality Control Checks and Procedures, 78, <https://www.ndbc.noaa.gov/publications/NDBCHandbookofAutomatedDataQualityControl2009.pdf>, 2009.
- Olson, J. B., Smirnova, T., Kenyon, J. S., Turner, D. D., Brown, J. M., Zheng, W., and Green, B. W.: A description of the MYNN surface-layer scheme, NOAA, <https://repository.library.noaa.gov/view/noaa/30605>, 2021.
- 830 Oost, W. A., Komen, G. J., Jacobs, C. M. J., and Van Oort, C.: New evidence for a relation between wind stress and wave age from measurements during ASGAMAGE, *Boundary-Layer Meteorology*, 103, 409-438, <https://link.springer.com/article/10.1023/A:1014913624535>, 2002.
- Pan, Y., Yan, C., and Archer, C. L.: Precipitation reduction during Hurricane Harvey with simulated offshore wind farms, *Environmental Research Letters*, 13, 084007, <https://iopscience.iop.org/article/10.1088/1748-9326/aad245>, 2018.
- 835 Petrović, V. and Bottasso, C. L.: Wind turbine optimal control during storms, *Journal of Physics: Conference Series*, 012052, <https://iopscience.iop.org/article/10.1088/1742-6596/524/1/012052>, 2014.
- Porchetta, S., Muñoz-Esparza, D., Munters, W., van Beeck, J., and van Lipzig, N.: Impact of ocean waves on offshore wind farm power production, *Renewable Energy*, 180, 1179-1193, <https://www.sciencedirect.com/science/article/pii/S0960148121012799>, 2021.
- 840 Porchetta, S., Temel, O., Muñoz-Esparza, D., Reuder, J., Monbaliu, J., Van Beeck, J., and van Lipzig, N.: A new roughness length parameterization accounting for wind–wave (mis) alignment, *Atmospheric Chemistry and Physics*, 19, 6681-6700, https://kuleuven.limo.libis.be/discovery/search?query=any,contains,LIRIAS2807444&tab=LIRIAS&search_scope=lirias_pr_ofile&vid=32KUL_KUL:Lirias&offset=0, 2019.
- 845 Porchetta, S., Temel, O., Warner, J. C., Muñoz-Esparza, D., Monbaliu, J., van Beeck, J., and van Lipzig, N.: Evaluation of a roughness length parameterization accounting for wind–wave alignment in a coupled atmosphere–wave model, *Quarterly Journal of the Royal Meteorological Society*, 147, 825-846, <https://rmets.onlinelibrary.wiley.com/doi/10.1002/qj.3948>, 2020.
- Powell, M. D. and Reinhold, T. A.: Tropical Cyclone Destructive Potential by Integrated Kinetic Energy, *Bulletin of the American Meteorological Society*, 88, 513-526, <https://journals.ametsoc.org/view/journals/bams/88/4/bams-88-4-513.xml>, 2007.
- 850 Pryor, S. C. and Barthelmie, R. J.: A global assessment of extreme wind speeds for wind energy applications, *Nature Energy*, 6, 268-276, <https://www.nature.com/articles/s41560-020-00773-7>, 2021.
- Pryor, S. C. and Barthelmie, R. J.: Power Production, Inter-and Intra-Array Wake Losses from the US East Coast Offshore Wind Energy Lease Areas, *Energies*, 17, 1063, <https://www.mdpi.com/1996-1073/17/5/1063>, 2024a.
- 855 Pryor, S. C. and Barthelmie, R. J.: Wind shadows impact planning of large offshore wind farms, *Applied Energy*, 359, 122755, <https://www.sciencedirect.com/science/article/pii/S0306261924001387>, 2024b.



- Pryor, S. C., Barthelmie, R. J., and Shepherd, T. J.: Wind power production from very large offshore wind farms, *Joule*, 5, 2663-2686, <https://www.sciencedirect.com/science/article/pii/S254243512100430X>, 2021.
- Riehl, H. and Malkus, J.: Some Aspects of Hurricane Daisy, 1958, *Tellus*, 13, 181-213, <https://onlinelibrary.wiley.com/doi/10.1111/j.2153-3490.1961.tb00077.x>, 1961.
- 860 Rose, S., Jaramillo, P., Small, M. J., Grossmann, I., and Apt, J.: Hurricane Risk to Offshore Wind Turbines Along the U.S. Coast, Carnegie Mellon University, <https://www.cmu.edu/ceic/assets/docs/publications/working-papers/ceic-12-01.pdf>, 2012a.
- Rose, S., Jaramillo, P., Small, M. J., Grossmann, I., and Apt, J.: Quantifying the hurricane risk to offshore wind turbines, *Proceedings of the National Academy of Sciences*, 109, 3247-3252, 865 <https://www.pnas.org/doi/full/10.1073/pnas.1111769109?doi=10.1073%2Fpnas.1111769109>, 2012b.
- Shchepetkin, A. F. and McWilliams, J. C.: The regional oceanic modeling system (ROMS): a split-explicit, free-surface, topography-following-coordinate oceanic model, *Ocean Modelling*, 9, 347-404, <https://www.sciencedirect.com/science/article/pii/S1463500304000484>, 2005.
- 870 Shchepetkin, A. F. and McWilliams, J. C.: Correction and commentary for “Ocean forecasting in terrain-following coordinates: Formulation and skill assessment of the regional ocean modeling system” by Haidvogel et al., *J. Comp. Phys.* 227, pp. 3595–3624, *Journal of Computational Physics*, 228, 8985-9000, <https://www.sciencedirect.com/science/article/pii/S0021999109004872>, 2009.
- Skamarock, W. C., Klemp, J. B., Dudhia, J., Gill, D. O., Liu, Z., Berner, J., Wang, W., Powers, J. G., Duda, M. G., Barker, D. M., and Huang, X.-Y.: A Description of the Advanced Research WRF Version 4, 162, 875 <https://opensky.ucar.edu/islandora/object/technotes%3A576>, 2019.
- Stewart, G. M. and Lackner, M. A.: The impact of passive tuned mass dampers and wind–wave misalignment on offshore wind turbine loads, *Engineering structures*, 73, 54-61, <https://www.sciencedirect.com/science/article/pii/S0141029614002673>, 2014.
- 880 Taylor, P. K. and Yelland, M. J.: The dependence of Sea Surface Roughness on the Height and Steepness of the Waves, *Journal of Physical Oceanography*, 31, 572-590, https://journals.ametsoc.org/view/journals/phoc/31/2/1520-0485_2001_031_0572_tdosr_2.0.co_2.xml, 2001.
- Tewari, M., Chen, F., Wang, W., Dudhia, J., LeMone, M. A., Mitchell, K., Ek, M., Gayno, G., Wegiel, J., and Cuenca, R. H.: Implementation and verification of the unified Noah land surface model in the WRF model (Formerly Paper Number 17.5), *Proceedings of the 20th Conference on Weather Analysis and Forecasting/16th Conference on Numerical Weather Prediction*, Seattle, WA, USA, 6 pp, https://ams.confex.com/ams/84Annual/techprogram/paper_69061.htm, 2004.
- 885 Valamanesh, V., Myers, A. T., and Arwade, S. R.: Multivariate analysis of extreme metocean conditions for offshore wind turbines, *Structural Safety*, 55, 60-69, <https://www.sciencedirect.com/science/article/pii/S0167473015000296>, 2015.
- Valamanesh, V., Myers, A. T., Hajjar, J. F., and Arwade, S. R.: Probabilistic Modeling of Joint Hurricane-induced Wind and Wave Hazards to Offshore Wind Farms on the Atlantic Coast, *International Conference on Structural Safety and Reliability (ICOSSAR)*, Columbia University, New York, NY, 890 https://people.umass.edu/~arwade/owt_hurricanes/valamanesh_myers_hajjar.pdf, 2013.
- Wang, J., Hendricks, E., Rozoff, C. M., Churchfield, M., Zhu, L., Feng, S., Pringle, W. J., Biswas, M., Haupt, S. E., Deskos, G., Jung, C., Xue, P., Berg, L. K., Bryan, G., Kosovic, B., and Kotamarthi, R.: Modeling and observations of North Atlantic cyclones: Implications for US Offshore wind energy, *Journal of Renewable and Sustainable Energy*, 16, 895 <https://pubs.aip.org/aip/jrse/article-abstract/16/5/052702/3316837/Modeling-and-observations-of-North-Atlantic>, 2024.
- Warner, J. C., Perlin, N., and Skillingstad, E. D.: Using the Model Coupling Toolkit to couple earth system models, *Environmental Modelling & Software*, 23, 1240-1249, <https://www.sciencedirect.com/science/article/pii/S1364815208000388>, 2008.
- 900 Warner, J. C., Armstrong, B., He, R., and Zambon, J. B.: Development of a Coupled Ocean–Atmosphere–Wave–Sediment Transport (COAWST) Modeling System, *Ocean Modelling*, 35, 230-244, <https://www.sciencedirect.com/science/article/pii/S1463500310001113>, 2010.
- Wiser, R., Rand, J., Seel, J., Beiter, P., Baker, E., Lantz, E., and Gilman, P.: Expert elicitation survey predicts 37% to 49% declines in wind energy costs by 2050, *Nature Energy*, 6, 555-565, <https://www.nature.com/articles/s41560-021-00810-z>, 2021.



- 905 Xie, L., Yan, T., Pietrafesa, L. J., Morrison, J. M., and Karl, T.: Climatology and Interannual Variability of North Atlantic Hurricane Tracks, *Journal of Climate*, 18, 5370-5381, <https://journals.ametsoc.org/view/journals/clim/18/24/jcli3560.1.xml>, 2005.
- Yihe, X.: 'Super typhoon' devastates wind farm on Chinese coast, RECHARGE, <https://www.rechargenews.com/wind/super-typhoon-devastates-wind-farm-on-chinese-coast/2-1-1706161>, 2024.
- 910 Zambon, J. B., He, R., and Warner, J. C.: Investigation of hurricane Ivan using the coupled ocean–atmosphere–wave–sediment transport (COAWST) model, *Ocean Dynamics*, 64, 1535-1554, <https://link.springer.com/article/10.1007/s10236-014-0777-7>, 2014a.
- Zambon, J. B., He, R., and Warner, J. C.: Tropical to extratropical: Marine environmental changes associated with Superstorm Sandy prior to its landfall, *Geophysical Research Letters*, 41, 8935-8943, 915 <https://agupubs.onlinelibrary.wiley.com/doi/full/10.1002/2014GL061357>, 2014b.